PROGRESS REPORT

on

STUDY OF THE PHYSICS OF LASER RADIATION

NASA Grant NGR-21-002-022

October 15, 1964 to October 15, 1966

UNIVERSITY OF MARYLAND
DEPARTMENT OF PHYSICS AND ASTRONOMY
COLLEGE PARK, MARYLAND

PROGRESS REPORT

on

STUDY OF THE PHYSICS OF LASER RADIATION

NASA Grant NGR-21-002-022

October 15, 1964 to October 15, 1966

Principal Investigator:

C. O. Alley

Associate Professor of Physics

Department of Physics and Astronomy

University of Maryland

College Park, Maryland

TABLE OF CONTENTS

Fiscal Report

REPRINTS OF PUBLICATIONS

REPRINTS OF PUBLICATIONS (con't)

ONSET OF LONG-RANGE ORDER IN A CRITICAL SOLUTION OF MACROMOLECULES
by J. A. White, J. S. Osmundson, and B. H. Ahn, Physical Review Letters 16, No. 1, 639 (1966)

DYNAMICAL COMPUTATION OF PHOTON CORRELATIONS AND COUNTING STATISTICS
by V. Korenman, submitted to the Physical Review

POLARIZATION AND ABSORPTION EFFECTS ON THE FRAUNHOFER DIFFRACTION PATTERNS OF A CORNER REFLECTOR
by C. O. Alley, R. F. Chang, D. G. Currie, and M. E. Pittman to be submitted to the Journal of the Optical Society of America

INTRODUCTION

This progress report describes research in quantum electronics involving the physics of laser radiation which has been made possible by NASA Grant NGR 21-002-022. It has provided the major support for the work on correlation effects in laser radiation, the exploitation of these effects in the scattering of laser light from fluctuations in optical media, studies on the propagation of short laser pulses, and optical radar measurements of micrometeorite density in the upper atmosphere. It has contributed significantly in the other areas described through the support of a research associate, a technician, a faculty research assistant, and a secretary for the group, whose services are shared by all members of the group. Other support for the research has been provided by the Advanced Research Projects Agency and by the Bureau of Ships. In a university research group it is neither possible nor desirable to compartmentalize completely the research supported by various agencies.

The grant has supported the summer salaries of two faculty members, honoraria and travel expenses for visiting physicists and seminar speakers, salaries of ten different graduate students for varying periods, five NSF summer students, and several part-time undergraduate research aides.

The stable laser research in the Electrical Engineering Department has benefited from the assignment of a physics graduate student to assist in the work in which we enjoy a close collaboration.

The design of the experiment on laser ranging to corner reflectors on the moon has not been explicitly supported by this NASA grant, but has benefited from the research environment the grant has helped to establish. It is included here because of its relation to the technology of optical space communication of interest to the Office of Advanced Research and Technology.

CURRENT RESEARCH PROGRAM

I. CORRELATION EFFECTS IN LASER RADIATION

Experiments are now under way in this laboratory to study the intensity fluctuations in light from a CW gas LASER operating in the threshold region, using single-photon counting and coincidence techniques to supplement analog correlation measurements. It has now been established by recent theoretical[1] and experimental developments[2] here and in other laboratories that interesting photon correlation effects are to be found just in this region of LASER operation.

The necessary electronic equipment has been constructed and assembled to permit preliminary measurements of optical intensity fluctuations over the time range 10^{-7} to 10^{-2} seconds. Initial tests on thermal sources indicate the equipment is performing as designed and that it can be applied to some measurements of LASER intensity

---

1. See for example the papers 3A-1 and 3A-2 presented at the 1966 International Quantum Electronics Conference in Phoenix, Arizona. Digests appeared in IEEE Journal of Quantum Electronics, QE-2, No. 4, April (1966). Selected papers from the conference are to appear in two early fall issues of the IEEE Journal of Quantum Electronics.

   "Theory of Noise in Solid-State, Gas, and Semiconductor LASERS", by H. Haken.
   "Quantum Noise and Amplitude Noise in LASERS", by M. Lax and W. H. Louisell.

   Similar matters were present for discussion at the 1966 Rochester Conference on Coherence and Quantum Optics by the same authors.

2. See for example the papers 1A-1 and 1A-2 presented at the 1966 Phoenix Conference (publication discussed above).

   "Photoelectron Statistics Produced by a LASER Operating below and above the Threshold of Operation", by C. Freed and H. A. Haus.
   "Observation of Photon Counting Distributions for Laser Light Below and Above Threshold", by A. W. Smith and J. A. Armstrong.

   Similar matters were presented for discussion at the 1966 Rochester Conference on Coherence and Quantum Optics by the same authors.

fluctuations.

Present efforts are devoted to the serious problem of stabilizing our CW laser in the threshold region against long-term drifts, a problem aggravated by the slow data acquisition rate of the present electronics. "Breadboard" circuitry and measurements of drift rates indicate that feedback circuits now under construction will satisfactorily stabilize our LASER in the critical threshold region. If the stabilization is successful, it will be due in great part to the stability of the gas discharge in the LASER tube we are using. The discharge tube uses the low-current-density aluminum electrodes designed by Dr. Hochuli of the University of Maryland, Department of Electrical Engineering,[1] and the discharge current is regulated to within a few parts per million at any value from 2-5 mA. by a control circuit constructed in this laboratory. We look forward to making measurements on one of the ultra-stable CW LASERS that Dr. Hochuli is now developing, in which the effects of cavity length changes will be greatly reduced even before feedback compensation.

A careful study of systematic effects and the experience of other investigators[2] have convinced us that the measurement of small effects in the threshold region of LASER operation eventually demands a more sophisticated data-recording system. Higher data-acquisition rates not only reduce the statistical uncertainties in the final measurements but also reduce the systematic errors introduced by the remaining small

---

1. "Cold Cathodes for Possible Use in 6328 Å Single Mode He-Ne Gas Lasers", by U. Hochuli and P. Haldemann, Rev. Sci. Instr. 36, 1493 (1965).

2. See Footnote No. 2, on Page 2

longterm drifts in operating point of the LASER. The design of such a system has been partially completed.

Well above threshold, a CW laser stabilized against long-term drifts provides a nearly monochromatic light source of essentially constant intensity. Such a source can then be used to study fluctuations in light scattered from or transmitted through a medium due to interactions with the medium itself. Our experience with stabilizing and measuring fluctuations in CW LASERS near threshold gives us the ability to produce and calibrate such a source. (See "Scattering from Fluctuations in Optical Media", Section II, below.)

II. SCATTERING FROM FLUCTUATIONS IN OPTICAL MEDIA

A. Application of Photo-Beat Techniques to the Measurement of Brillouin Scattering and Inelastic Rayleigh Scattering

Light scattered inelastically in solids and liquids can be studied by beating the light scattered from a LASER beam with itself or with part of the incident radiation in photoelectric detector. Studies of the application of this technique to Brillouin scattering in solids and liquids led to interest in a related subject: the diffusion broadening of LASER radiation scattered by concentration fluctuations near critical points associated with phase transitions in binary liquids.

In this laboratory Dr. J. A. White, Mr. J. S. Osmundson, and Mr. B. H. Ahn have been studying the fluctuations in light scattered from thermal fluctuations in fluids. Following this report, a copy of an article published in Physical Review Letters describes some of their measurements of light scattered from thermal fluctuations in the dielectric constant in a solution of macromolecules, using the Benedek method of self-beating

the scattered light in a square-law detector (a photomultiplier).

The same method applied directly to the output of a Spectra-Physics Type 115 He-Ne Laser provided upper limits on the lack of spectral purity in the light in a single laser mode (~3Hz.) and of the amplitude instability of the output, analyzed into its frequency components. In the process of striving for maximum signal/noise ratio in the scattering work and minimum interference from building vibrations, etc., many developments in vibration isolation, in improving the amplitude stability of the laser emission, and in eliminating spurious signals in the detection process were made.

One of the interesting unexpected results of the research, which was directed principally toward a greater understanding of critical phenomena, was the observation that relatively far from a critical point it seems to be possible to determine the diffusion velocity corresponding to the Brownian motion of individual molecules at least as small as 100 Å across. The light-scattering technique for studying diffusion in liquids will give information on the interactions of macromolecules of the same type as has been obtained for atomic diffusion from the scattering of neutrons. It will give previously unavailable information on the microscopic viscous interaction between a large molecule and its environment. (See, for example, the proceedings of various symposia on the Inelastic Scattering of Neutrons in Solids and Liquids, published by the International Atomic Energy Agency in Vienna, espicially the article "Neutron Scattering by 'Normal' Liquids" by P. G. de Gennes on p. 239 of the 1960 proceedings). Also light scattering with

high-intensity laser beams offers the possibility of measuring higher-order correlation functions of diffusion velocities.

Studies of the inelastic Rayleigh scattering are continuing to see how small molecules can be and still be discerned by the technique, and to study critical phenomena in other binary and pure fluids. Among pure fluids, xenon is being studied in an initial experiment, and some time will be spent on carbon dioxide, for checking our results against those of other investigators. It is anticipated that critical studies will be continued to other fluids, in order to get improved information on the role of intermolecular interactions on their dynamics.

Preliminary studies have been made of apparatus requirements for doing Brillouin scattering in these same and other materials. A small Fabry-Perot interferometer has been built and tested. It is planned to explore especially the possibility of using photo-beating methods in the Brillouin scattering, in order to obtain especially precise information of line spacings and widths, the former being determined by the velocity of hypersonic waves and the latter by the attenuation of these waves.

B. Photon Counting and Coincidence Measurements of Correlations in Inelastic Scattering of Light

When light from a monochromatic source of constant intensity (stable CW LASER) is scattered from fluctuating excitations in an optical medium, the correlations in the scattered electromagnetic field contain information about the fluctuations that is readily accessible to experimental measurement. Analog photo-beating techniques for studying inelastic Rayleigh scattering have already been discussed in the preceding

section. When characteristic fluctuation times are very short and intensities low, so that only a few scattered photons are available during the time for which a typical fluctuation persists, single photoelectron counting and coincidence techniques offer a convenient method of obtaining information about the fluctuations. Fast photoelectron-counting methods are being developed in this laboratory by Dr. R. Detenbeck and Mr. R. Chang. These will permit studies of short-time fluctuations in light scattered by transparent media. The use of fast n-fold coincidence techniques permits a convenient extension of the method of studies of higher-order correlations than the intensities (second order in amplitude) themselves.

One goal of the development is the study of fluctuations in light scattered by transparent media due to excitations of very short lifetimes (10^{-8}sec. or less). It has been suggested by A. L. Fetter[1] that intensity correlations in Raman-scattering light can be used to determine optical phonon life-times. No measurements of optical phonon lifetimes in the momentum region accessible to optical Raman scattering have yet been made, to the best of our knowledge.

Our initial equipment development has been directed towards less ambitious goals where photoelectron-counting techniques can make important immediate contributions to studies of the generation and propagation of laser light beams. In addition to studying the photon statistics of light from the laser itself the photon counting and coincidence techniques are about to be applied to measurements of diffusion of macromolecules. The difficulties encountered in extending the analog techniques to these measurements, short coherence times (of the order of 10^{-3} sec.) and low scattered intensities, lead naturally to the use of fast

---

1. A. L. Fetter, Phys. Rev. 139A, 1616 (1965).

photon-counting and coincidence techniques. We have developed equipment and techniques which greatly extend our abilities in this area.

The development of equipment for the photon-counting intensity-fluctuation experiments has been strongly influenced by our experience in the optical-radar atmospheric-scattering experiment. In the context of the single-photoelectron-counting requirements of the optical-radar experiment, 100 MHz circuitry made by both Chronetics (Nanologic series) and Edgerton Germeshausen and Grier (M100 series) was borrowed and evaluated. From these experiences there evolved a workable photon-counting system for the optical ranging and an indication of a "zero-order" system for the study of intensity fluctuations.

Instrumentation for the measurement of intensity-fluctuation correlations by photon-counting and coincidence techniques has been under development since the spring of 1966. Our preliminary system uses an RCA type 7265 photomultiplier and EG&G 100MHz counting equipment to measure the number of photoelectrons counted during a gating time T from a single phototube. Our analysis of this system, together with published measurements on newer phototubes indicates that this type of measurement is suitable for times T down to about 10^{-7} - 10^{-8} seconds. The electron collection time of the photomultiplier is the limiting factor. Since the counting time must be shorter than the coherence time of the field, other (coincidence) techniques are required to measure fluctuations of shorter characteristic times. The instrumentation can now make meaningful measurements with counting times T of one-half microsecond or more. This is adequate for studying fluctuations in laser radiation and for studying diffusion of macromolecules, although more sophisticated data-handling equipment is needed for the final measurements.

Additional work on the extension of these techniques to much shorter time scales is under way.

III. OPTICAL RADAR MEASUREMENT OF MICROMETEORITE DENSITY IN THE UPPER ATMOSPHERE

During the periods of October to December and February to April of the past year, a high power ruby laser and 20" telescope were used to measure the scattering cross-section of dust particles in the upper atmosphere as a function of height. Results of the first period were reported in Nature (see paper following). Before the second period, improvements were made to reduce the background noise and to extend the lower limit of the height range from 80 km to 60 km. The results of the second period showed marked improvement in these two respects and confirmed our first results. The results of the second period have not yet been reported. These will be combined with the results of a third run which is now in progress. One final improvement to the radar has been made which further reduces the background and which extends the lower height limit to 40 km. Although there is still some controversy in the literature as to the existence of these dust particles, we are confident of our results. This confidence is supported by recent in situ measurements of the particle size and the concentration of noctilucent clouds at 80 km.[1] A communication of this supporting evidence is being readied for publication.

---

1. Hemenway, Soberman, and Witt, Tellus 16, 84 (1964).

IV. STIMULATED ROTATIONAL RAMAN SCATTERING IN NITROGEN

The initial attempts to observe the stimulated Raman scattering from rotational levels of Nitrogen did not succeed due to the large beam divergence of the laser output. This is consistent with calculations of the threshold made by Dr. Alexander Glass (private communication). Attention was therefore placed on a study of the beam divergence and its reduction. Measurements showed that the present K2-Q produced a laser output with 90% of its output within a full angle of 20 milliradians for both of the available laser crystals. Doubling the length of the cavity halved this angle at the same output level. However, observation of the stimulated scattering appears to require a beam divergence of one milliradian or smaller. Thus additional means for obtaining the small beam divergence were sought. Two alternatives presented themselves. The straightforward approach of converting the K2Q to an amplifier-oscillator unit (K1500) which would provide the required beam was temporarily out of the question due to financial reasons and to the need for the K2-Q in the optical radar work.

The other approach tried was the use of the recently observed phenomenon of self-focusing[1] to increase the length of the beam within which a given power could produce the stimulated Raman effect. Although the threshold for self-focusing was lower than the power output of many lasers, the effect had not yet been seen or studied in air at one atm. Work was thus started to observe and make use of

---

1. Chiao, et al, Phys. Rev. Letters 13, 479 (1965).

this phenomenon in air. However, the K2-Q output proved also to be highly inhomogeneous in its spatial behavior. Correct location of diaphragms left a uniform beam, but one whose power was below the self-focusing threshold. No self-focusing effects were observed. To obtain the necessary uniform beam, we must again consider the conversion to an oscillator-amplifier laser system. Once this is done, further attempts to observe both the stimulated rotational Raman scattering and the self-focusing phenomenon will be begun.

V. PROPAGATION OF SHORT LASER PULSES

A. Precursor Waves

The relations of "precursor waves" to the signal velocities of light in various media, in the theory of Brillouin and Sommerfeld and its modern extensions, have been under study. The theories have been applied in detail to the problem of actually observing precursors experimentally in particular absorbing or amplifying (linear) media. With state-of-the-art techniques in fast single photon timing and present Q-switched or mode-locked LASERS, the precursor effects would be unobservably small in the cases so far considered. Analysis is continuing to ascertain the most general requirements for observable precursor waves and to discover an optical material in which the effect is observable with present techniques.

B. Generation of Short LASER Pulses

Experimental work has begun on a short-pulse generator consisting of a He-Ne LASER with an internal variable loss. Driven at the correct frequency, the internal loss serves to lock the many axial modes of the LASER, thereby producing short pulses (one nanosecond) as described by

Hargrave et al.[1] The variable loss device is an ultrasonically driven quartz block. The block and transducer have already been designed and purchased. They will shortly be placed within the optical cavity of a LASER which was constructed in our laboratory and mounted on a flat, vibration-free table built for this experiment.

We have two primary motivations for developing this type of short-pulse generator. Long-range plans include modification of the LASER to the ring type, and investigation of the effects of the variable-loss device in that configuration. More immediately, we are preparing to compare measurements of pulse lengths made by conventional and unconventional techniques in the nanosecond region where both are applicable. This comparison will aid in intepretation of measurements of ultrashort (picosecond) pulses, such as those reported by De Maria et al.[2] A crystal to generate the second harmonic of the laser line, which can be used to infer the width of even the ultrashort pulses, has been ordered. Also, a scanning Fabry-Perot interferometer has been assembled to measure the number of modes which are locked. Conventional means of measuring pulse widths in time can be applied to the same nanosecond pulses from the He-Ne LASER measured by the second-harmonic technique.

VI. DYNAMICAL COMPUTATION OF PHOTON CORRELATIONS AND COUNTING STATISTICS

A theoretical investigation is being made of the photon correlations

---

1. L. E. Hargrave, R. L. Fork, and M. A. Pollack, Applied Phys. Lettrs. 5, 4 (1964).

2. A. J. De Maria, D. A. Stetsen, and H. Heynau, Paper 4A-7 presented at the 1966 International Conference on Quantum Electronics at Phoenix Arizona. See the April 1966 issue of the IEEE Journal of Quantum Electronics, QE-2, No. 4, for a digest of the paper. Selected papers from the conference will be presented in full in fall 1966 issues of the same journal.

and photon-counting statistics in the electromagnetic field from arbitrary sources. The treatment is fully quantum-mechanical in the dynamic source-field interaction. Following this report is a copy of a paper just now being submitted for publication. Work is continuing on the applications of these techniques to several problems, including LASERS and the study of matter through its interaction with highly coherent light beams.

VII. INSTABILITIES AND MODE LOCKING PHENOMENA

A square ring He-Ne LASER of 5.5 meter periphery has been under study in this laboratory for many months. During the last few months we have constructed and studied the behavior of an even larger ring of 10 meter circumference, built on a stable foundation, operating in a controlled dust-free atmosphere, as a preliminary to construction of a 40 meter ring on the very stable floor of the presently unused cyclotron experimental area. The large ring LASERS offer promise as precision tools for the measurement of angular velocities and the Fresnel drag for light in moving media, if the mode interactions in these LASERS can be well understood. Our results with the 10 meter ring make it clear that the mode interactions, when the longitudinal mode spacing is smaller than the natural linewidth of the transition, offer a rich variety of interesting phenomena in themselves.

In the 5.5 meter ring contrarotating beams of equal intensity were stable, although their frequencies locked for small LASER rotation rates. In the 10 meter ring mode interactions lead to a new effect, a bistable condition in which either one or the other oppositely rotating components has nearly all of the total energy. The effect is ascribed to strong interactions among adjacent longitudinal modes, whose frequency separations in

the 10 meter LASER are smaller than the atomic linewidth.

The bistable effect is most pronounced at high power levels (~0.5 mW.). Additional evidence of strong adjacent-mode interaction is also observed in the behavior of this LASER at very low power levels. At low levels both beams are of equal intensity, but a fixed phase relationship among modes results in the production of short pulses. The mode-locked-pulse spacings at low power levels have been measured as 33, 16, and 11 nanoseconds under various operating conditions, corresponding to beats between adjacent longitudinal modes (30 MHz spacing), every second mode, and every third mode. At medium power levels the LASER is not quite bistable, alternating randomly between dominance by one direction or the other.

It is perhaps not surprising that different transverse modes, which use different spatial regions of the gas, do not compete. Even when operating in a bistable condition for the dominant TEM_{00} mode, the LASER may show a much weaker high-order-mode beam in the opposite direction from the main beam.

The 10 meter ring, operated on the very stable 6 foot thick concrete floor of the cyclotron experimental area, has been dismantled to make way for recent cyclotron construction. Additional space has been obtained on the concrete floor of the upper experimental room of the cyclotron complex, which will be available for LASER experiments for at least a year. Work has begun on construction in this place of the 40 meter ring laser, using an evacuated beam path. Many of the vacuum components (adjustable mirror boxes, etc.) have been completed, and leak testing and sealing is just being completed. The study of mode interactions will continue with this facility.

VIII. STABLE CW He-Ne GAS LASER

Associate Professor Urs Hochuli of the Department of Electrical Engineering is developing a highly stable (both frequency and amplitude) CW gas LASER, using a unique mounting for the cavity mirrors that minimizes thermal and vibrational length changes affecting cavity tuning. Most of the work is being carried out in the Electrical Engineering Department with ONR support, but some support has come from the NASA laser physics grant through Dr. Hochuli's close collaboration with our program.

In the LASER under development the mirror spacer is constructed of a low temperature-coefficient, thermally compensated ceramic material, suspended in a vacuum in a mounting similar to that devised by Drs. Weber and Zipoy of this department for their experiments on gravitational radiation. A cold-cathode DC discharge is used to excite the gas with minimum input power. The problem of developing cathodes which operate stably in the discharge over long periods of time has been solved.[1] Gas discharges have been operated for more than 14,000 hours and one has been "lasing" for more than 11,000 hours with a total gas volume of 30 cm^3. The application of these electrodes to He-Ne LASERS on a larger scale and to CO_2 LASERS is being studied.

The choice of a low-expansion ceramic material, for operation under electron and ion bombardment in the discharge without contamination of the gas, is an important objective of present research. Other factors affecting the stability of the gas discharge in a LASER (both long-term and short-term) are under study. Important among these is the control of plasma oscillations within the discharge.

---

1. U. Hochuli and P. Haldemann, Rev. Sci. Instr. 36, 1493 (1965).

IX. LASER RANGING TO OPTICAL RETRO-REFLECTORS ON THE MOON

Further detailed analyses of the scientific and technical aspects of this experiment have been made by the University of Maryland group and the co-investigators at several other universities. in an explicit proposal to NASA. These were:

Lunar Size and Orbit, by Dirk Brouwer, Yale University (Professor Brouwer died in January, 1966)

Motion of the Moon about its Center of Gravity, by Gordon MacDonald, UCLA

A Relativity Test, by R. H. Dicke, Princeton University

Geophysical Information Obtainable from Lunar Distance Measurements, by P. L. Bender, Joint Institute for Laboratory Astrophysics of NBS and University of Colorado

Requirements for Frequency of Observation by Laser Tracking of the Moon, by W. M. Kaula, UCLA

Signal to Noise Analysis, by H. Richard (Goddard Space Flight Center), S. K. Poultney and C. O. Alley, University of Maryland.

Design and Testing of Lunar Retro-reflecting Systems, by J. E. Faller, Wesleyan University.

Discussion of Short Pulse Ruby Laser System, by S. K. Poultney and C. O. Alley, University of Maryland

The experiment has received the strong endorsement of NASA Headquarters, and some initial funding has been provided. It is hoped that the measurements can be begun with the first Apollo landing. The Perkin-Elmer Company is now under subcontract to the University of Maryland to assist in the optical design of the experiment. Tests have been completed to establish the predicted performance of 1 1/2" solid fused silica corner reflectors in the simulated lunar environment using a space simulator at the Goddard Space Flight Center.

The far-field diffraction pattern of a corner reflector has been studied theoretically (for arbitrary phases and amplitudes at each reflection) and experimentally (for several types of reflecting surfaces). The investigation is

motivated by the possibility of "optical radar" range measurements using corner reflectors on the moon and a LASER transmitter on the earth. Quantitative information on the concentration of the return signal is of great importance in the system design.

Exact expressions have been obtained for the amplitudes of both polarization components in the far-field diffraction pattern of a corner illuminated by a linearly polarized axial beam. Computer calculations of intensity patterns for a wide choice of corner parameters (arbitrary in the general theory) are under way.

JOURNAL OF GEOPHYSICAL RESEARCH Vol. 70, No. 9 MAY 1, 1965

Optical Radar Using a Corner Reflector on the Moon

C. O. ALLEY,[1] P. L. BENDER,[2] R. H. DICKE,[3] J. E. FALLER,[2] P. A. FRANKEN,[4] H. H. PLOTKIN,[5] AND D. T. WILKINSON[3]

In a recent letter *Hunt* [1964] described a microwave transponder that can be landed on the moon and that can be used, in conjunction with a modified Glotrac station, to measure the distance between station and landing site. He also suggests several interesting measurements that could be made on the earth-moon system if the range accuracy were sufficiently well developed. The purpose of this letter is to point out the capabilities and possible advantages of an optical radar system which uses a corner reflector on the moon's surface.

Smullin and Fiocco [1962] have demonstrated that laser beams can be scattered from the moon's surface and detected back at the earth; however, the return signals were too weak and too spread out (in time) to be used for precision ranging. *Hoffman et al* [1960] have pointed out the advantages of using corner reflectors on an artificial satellite to permit precision tracking. More recently, *Plotkin* [1964] has described an optical radar system that is capable of making precision range measurements to satellites which have been equipped with corner reflectors.

A typical optical radar system is shown schematically in Figure 1. The laser beam (pulsed or continuous wave) is sent through a transmitting telescope which tracks the corner reflector on the moon's surface. A small part of the reflected light is collected by the receiving telescope, which also tracks the reflector. (If a single telescope with a T/R switch is used, there is some sacrifice of received intensity owing to velocity abberation.) The correlator measures the light travel time to the reflector and back. The efficiency of such a system, that is, the ratio of the number of received to the number of transmitted photons, is given approximately by

$$\eta = \frac{1}{4}\frac{A^2 D_T^2 D_R^2}{r^4\theta^2\lambda^2 D_L^2} T_a^2 T_s$$

where

A is effective area of the corner reflector, $\approx$150 cm^2.
r is range to the corner reflector, $\approx 3.7 \times 10^{10}$ cm.
λ is wavelength of laser light, $\approx 7 \times 10^{-5}$ cm.
θ is angular radius of laser beam divergence, $\approx 10^{-3}$ rad.
D_R is diameter of receiving telescope, $\approx$100 cm.
D_T is diameter of transmitting telescope, $\approx$100 cm.
D_L is diameter of laser rod, $\approx$2 cm.
T_a is transmission through the atmosphere, $\approx$85%.
T_s is transmission through optical elements, $\approx$30%.

For a system having the parameters given above, the efficiency is $\approx 3.3 \times 10^{-18}$; thus, we see the need for a high power laser as the light source. The expected return from the corner reflector is some 100 times stronger than that due to diffuse scattering by the lunar surface.

For pulsed radar applications, a Q-switched ruby laser can be used as the light source. The parameters used above for estimating η are typical of a system employing a ruby laser which is available commercially and is capable of delivering 10^{19} photons in a pulse of 10^{-8} second duration. With this laser as the light source and with a detector of 3% quantum efficiency, we estimate a return signal of 1 photoelectron per transmitted pulse. Therefore, the probability of getting a return signal from a given trans-

[1] Department of Physics, University of Maryland, College Park, Maryland.
[2] Joint Institute for Laboratory Astrophysics, Boulder, Colorado.
[3] Palmer Physical Laboratory, Princeton University, Princeton, New Jersey.
[4] Department of Physics, University of Michigan, Ann Arbor, Michigan.
[5] Goddard Space Flight Center, National Aeronautics and Space Administration, Greenbelt, Maryland.

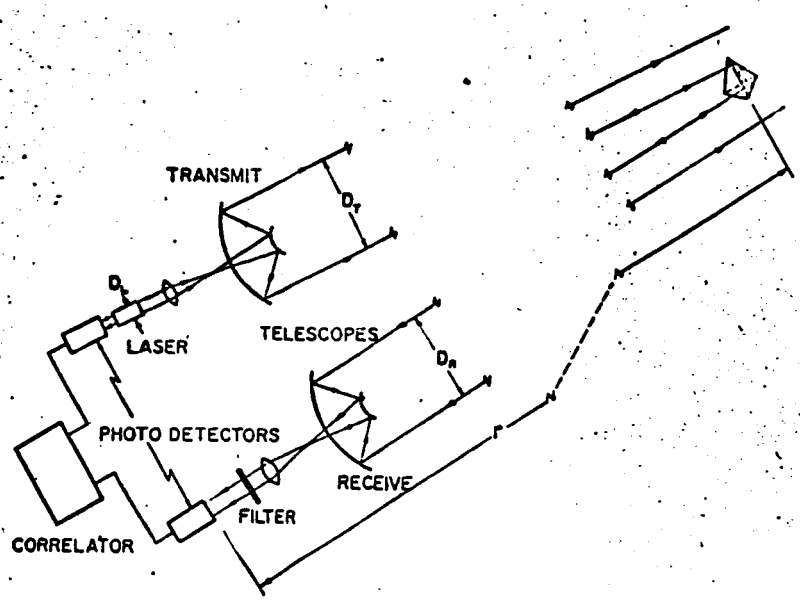

Fig. 1. A typical optical radar system.

mitted pulse is quite high. Furthermore, each measured return gives the light travel time to the corner reflector and back with an accuracy of 10^{-4} second (4 parts in 10^9).

Background noise in the receiver comes mostly from sunlight which has been scattered from the moon's surface or from the earth's atmosphere. The estimated background noise for the system described above and for the corner reflector in sunlight is 10^6 photoelectrons per second for a 10 A optical bandwidth. However, the effective signal to noise ratio can be enhanced by gating the receiver output with a pulse whose turn-on time is controlled by ephemeris predictions and whose width is sufficient to cover uncertainties in the ephemeris. Background noise and uncertainties in the gating ephemeris are such that the return signal would have to be located initially by nighttime observations of a corner reflector on the dark part of the moon. However, these measurements could be used to improve the gating ephemeris and reduce the gate width to the point where ranging to a sunlit corner reflector would be possible. The nature of the major uncertainties that occur in the gating ephemeris are such that this improvement would go rapidly.

The corner reflector and its mounting must be designed carefully in order to avoid environmental problems on the moon's surface. Large temperature excursions, damage from radiation, and the possibility of dust being cast up by the vehicle landing are some of the problems that must be considered. If the corner reflector is mounted atop a soft-landing vehicle whose destination is near the center of the moon's disk, then an orientation mechanism is not required. For vehicles landing far from the disk center, the corner reflector would need to be reoriented after landing or, alternatively, an array of corner reflectors could be used. An effective area of 150 cm^2, which was used in our estimation of η, corresponds to a corner reflector, of the type described by Hoffmann et al., with an edge length of 16.2 cm and with optimum orientation. This corner reflector, exclusive of the mounting, would weigh about 1.5 kg if made of solid quartz, and less if made from orthogonal plane mirrors.

The passivity and the expected reliability of the corner reflector and the high accuracy of the optical ranging seem to be the chief advantages of this system over the transponder system described by Hunt.

The optical radar system could be used to obtain important information in several fields of study. A few interesting measurements are listed below.

1. Lunar size and orbit. A comparison of the measured and theoretical range over long pe-

riods of time can be used to measure the radius of the moon at the corner reflector position and, also, to give an accurate check on lunar orbit theory.

2. Geodesy. Simultaneous ranging by several stations, with known geographical positions, could be used to measure the size and shape of the earth. Also, a connection could be established between the American and European geodesic networks.

3. Lunar librations. With three or more corner reflectors on the moon, whose ranges could be measured simultaneously from a single radar station, the amplitudes and periods of the lunar liberations could be measured with high accuracy.

4. Reckoning of ephemeris time. After the librations have been measured, a corner reflector could be used as a fiducial point to be located with respect to the star background for purposes of reckoning ephemeris time.

5. Improvement of landing site location. The returning laser light has essentially been reflected from a point on the moon's surface. This should permit accurate location of the corner reflector, relative to known surface features, by photographic and/or photoelectric techniques.

6. Gravitational waves. A long time series of range measurements could be searched for disturbances or periods which are not explained by the perturbations contained in the lunar theory. Such effects, if seen, might be identified with gravitational wave effects.

The caliber of the measurements in this list seems to us to warrant a careful consideration of the problems involved in including corner reflectors on some of the lunar vehicles now being planned.

References

Hoffmann, W. F., R. Krotkov, and R. H. Dicke, *IRE Trans. Military Electron., 4*, 28, 1960.

Hunt, M. S., A prototype lunar transponder, *J. Geophys. Res., 69*, 2399, 1964.

Plotkin, H. H., *Quantum Electronics 3*, Vol. 2, p. 1319, Columbia University Press, New York, 1964.

Smullin, L. D., and G. Fiocco, *Proc. IRE, 50*, 1703, 1962.

(Received December 3, 1964.)

(*Reprinted from Nature, Vol. 209, No. 5025, pp. 798–799, February 19, 1966*)

Optical Radar Detection of Backscattering from the Upper Atmosphere (75–160 km)

AN optical radar system has recently been used to detect and study backscattering from the upper atmosphere (75–160 km). Although a much more detailed investigation is in progress, our preliminary results seem to indicate rough agreement with those of Fiocco and Smullin[1]. These authors suggested micrometeorites as a source of the echoes. When observations were made for brief time intervals (0·5 h or less), peaks were sometimes observed in the return-signal profiles. It should be noted, however, that when averaged over a period of several hours the return signal tends to become relatively smooth. It would seem, therefore, that the altitudes of the scattering layers, if they exist, fluctuate rapidly with time. The total scattering cross-section at 6943 Å observed by us is of the same order of magnitude as that reported by Fiocco and Colombo[2] ($\overline{N\sigma} \approx 10^{-12}$ cm^{-1}).

The optical radar consists of a Korad K-2Q ruby laser which is capable of producing single pulses containing 6–10 J at 6943 Å with a width of 10 nsec and a beam divergence of no more than 10 milliradians. The ruby is 8 in. long, 5/8 in. in diameter and is surrounded by a helical flash lamp. Q-spoiling is achieved by means of a Kerr cell. The laser pulse is brought to a focus at a 1/8 in. diameter aperture in a rotating mirror. The aperture is located in the focal plane of the University of Maryland's 20-in. reflector, which is a Broken Cassegrain with a 300-in. effective focal length. The beam divergence of the light leaving the telescope is less than 0·4 milliradians. In order to prevent air breakdown, the rotating mirror is installed in a chamber which is evacuated to a pressure of about 10μ mercury. An average energy of 1·0 J per pulse was sent into the atmosphere. Each laser pulse was monitored for proper firing time and for pulse amplitude. The return signal from the telescope is reflected by the rotating mirror to the cathode of a cooled E.M.I. 9558B photomultiplier tube (S-20 cathode) which is gated off during the actual laser firing. A 10 Å pass-band interference filter was used in the experiment.

Due to the small magnitude of the signal, the experiment consists of counting individual photoelectrons. The pulses are processed by Chronetics Nanologic Modules and sent through logic circuits[3] to an 'on-line' *CDC* 160 computer which is programmed[3] to store the counts from each altitude interval. At present the system is capable of obtaining an atmospheric scattering profile, for each laser pulse, with an altitude resolution of 2·5 km.

All measurements were made at College Park, Maryland (76° 57′ W. long., 39° N. lat.), while looking at the zenith.

Figs. 1 and 2 give the results for two nights out of five for which we have obtained data. Fig. 1 shows the result of a series of shots taken during a short time interval. The scattering appears to be enhanced over the altitude ranges from 100 to 125 km. The total number of counts received (in 10 pulses) from 75 to 150 km was 2,240. The background was 350 counts. The number of photoelectrons due to backscattering is thus 1,890 with a mean

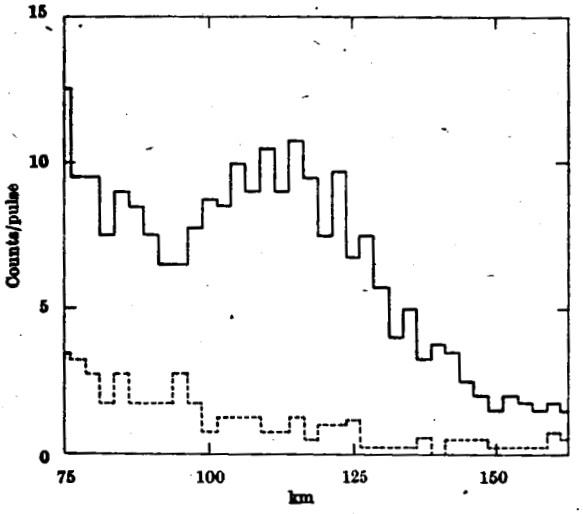

Fig.1. October 29, 1965, 07h 30m—08h 00m U.T. ——, Observed return (average of ten laser pulses); – – – –, background (average of ten laser pulses)

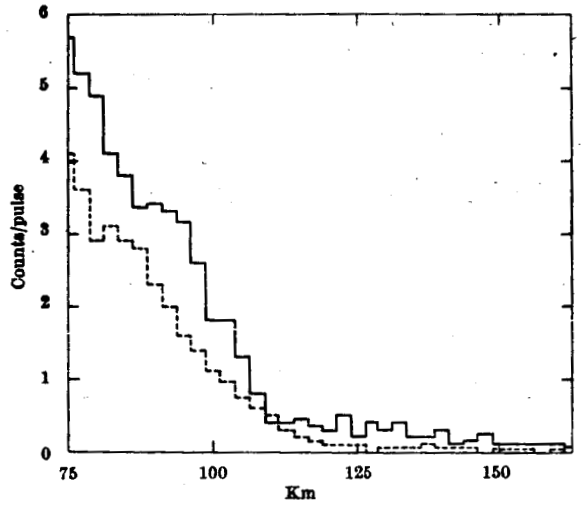

Fig. 2. October 31, 1965, 05h 30m– 09h 30m U.T. ——, Observed return (average of one hundred laser pulses); – – – –, background (average of twenty laser pulses). (Note change of vertical scale from that of Fig. 1)

error of 51 due to statistical uncertainty. Fig. 2 is the average of 100 laser pulses, over a period of 4 h, on a different night. The magnitude of the return signal is much lower than in Fig. 1 and no peaks are present. For the range 75–150 km we have: a total return of 5,070 counts, a background of 3,330 counts, a backscattering of 1,740 counts with a mean error of 147 counts. The high background is due to the fact that we use the same optical path for both transmitting and receiving. It is difficult to shield the phototube completely from the high light-levels present and from ruby fluorescence. Background measurements were made, during observations, by placing a black cloth over the end of the telescope tube.

We thank Prof. S. F. Singer for his encouragement and advice. This work was supported, in part, by the U.S. Weather Bureau under grant *WBG–4–FY–64* Advanced Research Projects Agency contract *SD–101*, National Aeronautics and Space Administration grant *NGR* 21–002–022 and Bureau of Ships contract *NObsr* 72710.

P. D. McCormick
S. K. Poultney
U. Van Wijk
C. O. Alley
R. T. Bettinger

Department of Physics and Astronomy,
University of Maryland.

J. A. Perschy

Applied Physics Laboratory,
Johns Hopkins University.

[1] Flocco, F., and Smullin, L. D., *Nature*, **199**, 1275 (1963).
[2] Flocco, F., and Colombo, G., *J. Geophys. Res.*, **69**, 1795 (1964).
[3] Perschy, J., M. S. Thesis, Univ. Maryland (1965).

Printed in Great Britain by Fisher Knight & Co., Ltd., St. Albans.

Reprinted from THE REVIEW OF SCIENTIFIC INSTRUMENTS, Vol. 36, No. 10, 1493–1494, October, 1965
Printed in U. S. A.

Cold Cathodes for Possible Use in 6328 Å Single Mode He-Ne Gas Lasers*

U. HOCHULI AND P. HALDEMANN
University of Maryland, College Park, Maryland 20742

(Received 9 April 1965; and in final form, 15 June 1965)

Properly dimensioned aluminum cold cathodes promise single mode 6328 Å He-Ne gas laser lifetimes exceeding 3000 h with total gas volumes of only 50 cm³. These cathodes are simple, rugged, and require only about 0.5 W for an emission current of 5 mA dc. Beryllium cold cathodes may be even better but more time is needed for their evaluation.

THE single mode 6328 Å gas laser usually works with a 5 to 1 He-Ne gas mixture under a total pressure of 3 Torr. With dc excitation the voltage drop across the 1 mm capillary discharge tube of 5 cm length is approximately 450 V for a current of 5 mA. Cold cathodes, having a cathode drop of about 100 V, require only half a watt for the emission of 5 mA. They become very attractive if the following conditions can be met: (a) yield a lifetime of several thousand hours with a total gas volume of 50 cm³; (b) very low deposits due to sputtering; and (c) reasonably constant voltage drop and gas mixture ratio over its lifetime.

Suitable cathode surfaces usually considered can be divided into 3 groups: (1) earth alkali oxide coated surfaces such as BaO layers used in neon sign electrodes; (2) metals such as Mo, or Nb, or Zr that give very reliable cathode falls once the surfaces are sputtered clean[1,2]; (3) metals such as Al, Mg, or Be that have thin oxide films.

None of our test discharges from cathodes in the first two groups listed had a longer life than about 500 h under the conditions given.

It is well known that electrodes of group 3 have a low sputtering rate as long as the oxide films are present.[3,4] To preserve the oxide layer we have tried to reduce the current density by avoiding hollow cathodes with small diameters. The results are shown in Table I.

TABLE I. Discharge life for different cathode diameters d, $p \simeq 3$ Torr He–Ne 5:1, $I = 5$ mA dc, gas volume $\simeq 50$ cm³.

Diameter in mm	Lifetime Mg	Lifetime Al	
3.2		24 h	
7.0		190 h	
11.5	1500 h	>3000 h	see Fig. 3
16.0		>3000 h	
22.0		>3000 h	

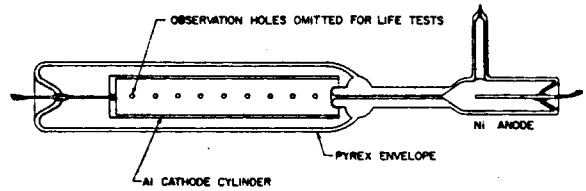

FIG. 1. Cross section of a typical discharge tube.

* Supported in part by the U. S. Office of Naval Research and the Advanced Research Project Agency.

[1] F. M. Penning, J. H. A. Moubis, and T. Jurriaanse, Philips Res. Rept. 1, 119, 225, 407 (1946).
[2] A. D. White, J. Appl. Phys. 30, 711 (1959).
[3] W. Espe and M. Knoll, *Werkstoffkunde der Hochvakuumtechnik* (Springer, Berlin, 1936), pp. 77 and 81.
[4] P. D. Kueck and A. K. Brewer, Rev. Sci. Instr. 3, 427 (1932).

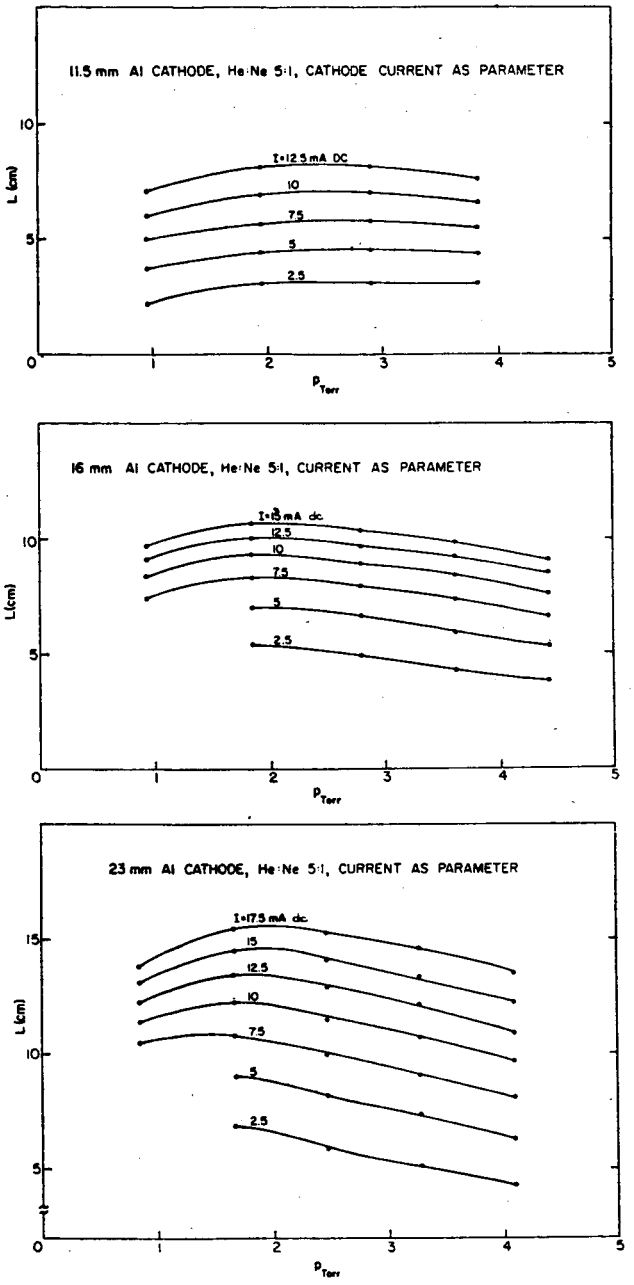

FIG. 2. Cathode glow length vs total pressure p.

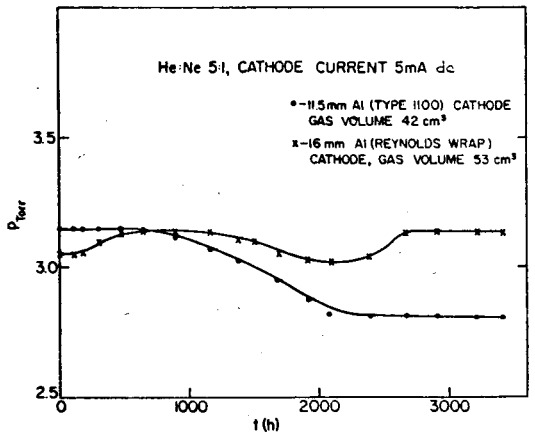

FIG. 3. Pressure vs time.

Figure 1 shows the cross section of a typical discharge tube. Figure 2 gives the length of electrodes covered with the cathode glow as seen by visual inspection through small holes along the cathodes.

Figure 3 shows pressure-time curves for two different electrode diameters.

The fact that the intensity ratio of the 6402 Å Ne and 3888 Å He lines stayed practically the same for the 11.5 end 16 mm electrodes is an indication that the composition of the gas mixture was approximately constant over a period of 3000 h. The total discharge voltage variation stayed within 30 V over this period of time.

Life tests on 22 mm Al cathodes and on an 18 mm Be cathode are being conducted but it may take several thousand hours before any firm conclusions can be drawn.

An 11.5 mm Al electrode has been used in an actual laser and has so far given satisfactory service for 3000 h with a gas volume of 30 cm³. This laser had a ^{3}He:^{20}Ne isotope filling and the total discharge voltage stayed within 10 V over this period of time.

Note added in proof. The pressure of the 11.5 mm test electrode was 2.65 Torr after 6300 h, and the laser was still working satisfactorily after 4500 h. The 16 mm electrode died after 4000 h, indicating that Reynolds wrap is not performing as well as type 1100 Al.

Reprinted from THE REVIEW OF SCIENTIFIC INSTRUMENTS,
Vol. 37, No. 6, 808, June, 1966
Printed in U. S. A.

Cold Cathodes for Possible Use in 6328 Å Single Mode He-Ne Gas Lasers

[Rev. Sci. Instr. 36, 1493 (1965)]

U. HOCHULI AND P. HALDEMANN
University of Maryland, College Park, Maryland 20742

(Received 11 March 1966; and in final form, 30 March 1966)

CHEMICAL analysis showed that the 3.2, 7, and 11.5 mm cold cathodes are of the type 2024 aluminum and not of type 1100 as indicated.

ONSET OF LONG-RANGE ORDER IN A CRITICAL SOLUTION OF MACROMOLECULES*

J. A. White, J. S. Osmundson, and B. H. Ahn

University of Maryland, College Park, Maryland

(Received 4 March 1966)

Diffusion broadening has been observed in the inelastic scattering of monochromatic light off a binary fluid, cyclohexane-polystyrene, near its critical point for mixing. The broadening a few tenths of a degree above the critical temperature is an order of magnitude less than in a binary mixture of small molecules (cyclohexane-aniline)[1] and two orders of magnitude less than in a pure fluid (SF_6).[2] The dependence of the broadening on scattering angle agrees with that found for the other fluids,[1,2] and with expectation[3]; but its increase with rising temperature is less rapid than for these fluids, being less than linear in ΔT.

The method used was substantially that of Benedek.[4,2] A 12-mm diameter cylindrical sample of cyclohexane containing 6.5% by volume National Bureau of Standards standard 705 polystyrene, with narrow molecular-weight distribution,[5] was irradiated with monochromatic light at 6328 Å from a He:Ne laser. Light scattered at an angle θ with respect to the incident direction was detected at a photomultiplier, where interference between the different frequency components in the scattered light produced a fluctuating photoemission. The noise spectrum of the amplified photocurrent, with dc component suppressed, was analyzed into its frequency components using a spectrum analyzer (Nelson-Ross type 011) with a resolution of 10 Hz.

Photographs of typical spectra are displayed in Fig. 1. Each photograph shows the digitized average of the noise amplitudes obtained in about 100 sweeps through the spectrum, each of 8 sec duration. An ND-800 Enhancetron

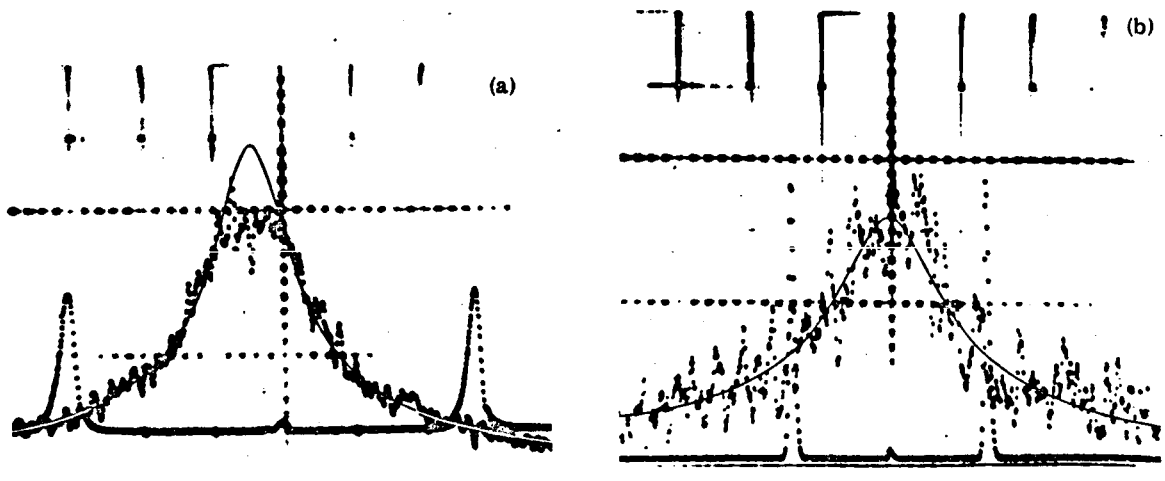

FIG. 1. Oscilloscope traces of digitized and time-averaged spectra of noise currents produced by the inelastically scattered light. (a) $\theta = 40°$, $T - T_S = 0.3°C$, marker pips at ±150 Hz. (b) $\theta = 80°$, $T - T_S = 4.0°C$, marker pips at ±1000 Hz. The solid curves are square-root Lorentzians fitted to the data. Suppression of low-frequency components and some drift of the heterodyne frequency of the spectrum analyzer account for the depression in the center of the narrower spectrum [part (a)]. Spectra obtained at $\theta = 20°$ and $\Delta T < 2°C$ are about as clean as that in (a), though narrower for small ΔT and therefore more susceptible to drift.

was used to perform the average.

The noise spectra have approximately square-root Lorentzian shape, as found for a pure fluid by Benedek and Ford,[2] and as required[2] for a Lorentzian spectrum of optical frequencies in the scattered light. The observed shape is consistent with exponential relaxation[3] of the fluctuations in concentration responsible for the inelastic scattering.

Assuming the scattered light has Lorentzian profile, its spectral width, or the reciprocal of the relaxation time multiplied by π, is equal to the half-width at half-amplitude of the detected noise current, divided by $\sqrt{3}$. (The noise current is proportional to the square root of the noise energy; the spectrum of the latter is Lorentzian, with half-width equal to the full width of the spectrum of the scattered light.[2]) The spectral widths deduced in this way from the observed noise amplitudes are displayed in Fig. 2. The data are for scattering angles of 20°, 40°, 80°, and for temperatures 0.05 to 30°C above the temperature $T_S = 24.28$°C $\approx T_{crit}$ at which the phases separated. The data may be represented approximately, as indicated by the solid lines in Fig. 2, by the semiempirical equation

$$\Delta\nu = 2.6[(2\pi/\lambda)\sin(\theta/2)]^2(T-T_S)^{0.6}\ \text{Hz}, \qquad (1)$$

in which $\lambda = 0.44$ is the wavelength of the light in the fluid, expressed in microns. In this equation the angular dependence is that expected theoretically for isotropic diffusion[3]; the coefficient 2.6 and the exponent in the temperature factor have been chosen arbitrarily. (They best fit the data for $\theta = 20°$ and $T-T_S < 16$°C.)

Although the agreement is not perfect, it is evident that the observed broadening conforms at least approximately to the $\sin^2(\theta/2)$ dependence expected theoretically. The observed dependence of the broadening on temperature, however, is not even approximately represented by linearity in $T-T_{crit}$, as expected on classical theory for small molecules[3] and shown by the dotted line in Fig. 2; rather, the breadth of the scattered line increases significantly less rapidly than linearly, the proportionality being more nearly to the square root of $T-T_S$.

No striking deviation from linearity in $T-T_S$ was observed for the intensity (dc component) of the scattered light. Within the range 0.1-2°C above T_S the reciprocal intensity was found to vary approximately (within ~10%) as $2+17(T-T_S)$, $3.5+24(T-T_S)$, $5+20(T-T_S)$, in arbitrary units, at $\theta = 20°, 40°, 80°$, respectively.[6] The over-all dependence,

$$\Gamma^{-1}(\theta, T) = C(\theta)[0.38\sin^2(\theta/2) + (T-T_S+0.1)], \qquad (2)$$

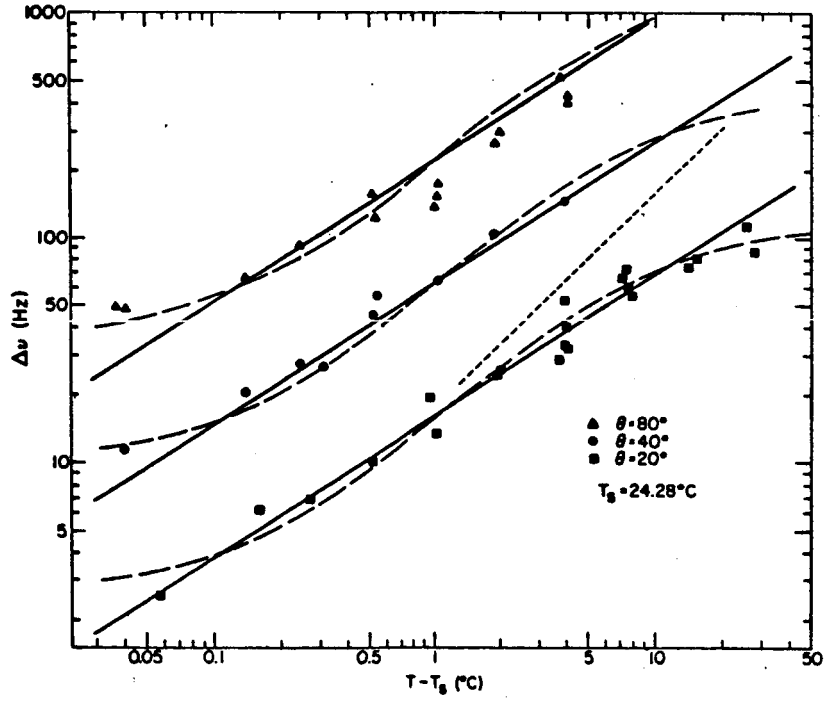

FIG. 2. Spectral width of the scattered light as a function of temperature and scattering angle. Dotted line indicates linearity in $T-T_S$. Solid lines are given in Eq. (2), dashed curves by Eq. (3).

agrees with that predicted by Debye[7] for a critical mixture with critical temperature $T_{crit} = T_S - 0.1°C$.[8]

Some decrease in the rate of growth of the spectral width of the scattered light can be expected at high temperatures, owing to the limit on disorder imposed by the finite extent of individual polymer molecules. These molecules, of average molecular weight $M = 180\,000$,[5] at infinite dilution have an end-end extension given by the empirical relation $L^2 \approx 0.47M$ (Å^2),[9] or radius of gyration $r = L/\sqrt{6} \approx 120$ Å. From the observations of Cummins, Knable, and Yeh[10] of the broadening for somewhat larger latex spheres suspended in dilute solution in water, the limiting breadth due to Brownian diffusion of spheres of this radius in cyclohexane (with viscosity 0.6 that of water) is found on extrapolation to be ~250 Hz for $\theta = 20°$, and larger in proportion to $\sin^2(\theta/2)$ for the other angles. The value thus estimated is considerably larger at $\theta = 20°$ than the ~100 Hz which seems to be approached experimentally at this angle at high T. The estimate is a crude one, however, and probably gives too large a value for the Brownian diffusion, and hence for the linewidth, as it neglects interactions between the polymer molecules. Such interactions are certainly significant in the nondilute solution used in our investigations.[11]

It is tempting, in view of the possible offset of T_{crit} from T_S and approach to a limiting $\Delta\nu$ at high T, to try to reanalyze the data in Fig. 2 assuming that the breadth at first increases linearly with $T - T_{crit}$, $T_{crit} \neq T_S$, then, far from T_{crit}, approaches a constant limiting value. If these features are combined by modifying Eq. (1) to read as follows:

$$\Delta\nu = 2.6\left(\frac{2\pi}{\lambda}\sin\frac{\theta}{2}\right)^2 \frac{T - T_c}{1 + 0.13(T - T_c)}\ \text{Hz}, \qquad (3)$$

with $T_c = T_S - 0.15$, then as good a fit to the data is obtained (dashed curves in Fig. 2) as with Eq. (1). The offset assumed here, $T_S - T_{crit} = 0.15°C$, is consistent with that used in Eq. (2). The limiting breadth,

$$\Delta\nu \to 20\left(\frac{2\pi}{\lambda}\sin\frac{\theta}{2}\right)^2 \text{Hz},$$

is not much greater than the breadth found experimentally at $T = 50°C$.[12]

In conclusion, the authors wish to thank Dr. D. McIntyre of the National Bureau of Standards for lending them the sample of polystyrene used in this experiment,[6] and Dr. C. O. Alley, Jr., of the University of Maryland for the opportunity to do this work in his quantum electronics laboratory.

---

*Work supported in part under Advanced Research Projects Agency Contract No. SD-101 and National Aeronautics and Space Administration Grant No. NGR 21-002-022.

[1] S. S. Alpert, Y. Yeh, and E. Lipworth, Phys. Rev. Letters 14, 486 (1965).

[2] N. C. Ford, Jr., and G. B. Benedek, Phys. Rev. Letters 15, 649 (1965).

[3] Cf. P. Debye, Phys. Rev. Letters 14, 783 (1965).

[4] G. B. Benedek, paper presented at the Proceedings of the Conference on Phenomena in the Neighborhood of Critical Points, National Bureau of Standards, Wahington, D. C., 1965 (to be published); Ford and Benedek, Ref. 2.

[5] A certificate describing Standard Sample 705 Polystyrene is available from the National Bureau of Standards, Washington, D. C. 20234. Number- and weight-average molecular weight determinations made at the National Bureau of Standards gave values within ±6% of the nominal $M = 180\,000$.

[6] More extensive measurements of the scattered intensity have been made at the National Bureau of Standards; cf. D. McIntyre and A. M. Wims, paper presented at the Proceedings of the Second Interdisciplinary Conference on Electromagnetic Scattering, Amherst, Massachusetts, 1965 (to be published).

[7] P. Debye, J. Chem. Phys. 31, 680 (1959).

[8] From the ratio of the coefficients of the θ and T terms in Eq. (2), a Debye interaction range, or effective coil size, $l = 30$ Å can be calculated, in agreement with the results of P. Debye, H. Coll, and D. Woermann, J. Chem. Phys. 33, 1746 (1960).

[9] N. T. Notley and P. J. W. Debye, J. Polymer Sci. 17, 99 (1955).

[10] H. Z. Cummins, N. Knable, and Y. Yeh, Phys. Rev. Letters 12, 150 (1964).

[11] The viscosity at $T = 50°C$ near the critical concentration for $M = 180\,000$ is probably nearly an order of magnitude larger than for pure cyclohexane at the same temperature [cf. P. Debye, B. Chu, and D. Woermann, J. Polymer Sci. A1, 249 (1963)]. The decreased rate of diffusion which might be concluded from this greatly increased viscosity may be offset to some extent by a decrease in molecular extension. P. Debye, B. Chu, and D. Woermann [J. Chem. Phys. 36, 1803 (1962)] have inferred from the angular dissymetry in the intensity of light scattered at critical concentration that the end-end separation in polystyrene at this concentration is $\sim\frac{1}{3}$ that at infinite dilution for $M = 2.8 \times 10^6$; Debye, Coll, and Woermann, Ref. 8, have found a somewhat less than three-fold in size decrease for $M = 10^6$.

[12] Equation (3) should not be assumed to apply for temperatures much above those used in our experiments.

For example, over large intervals of temperature noncompensating changes in viscosity and molecular extension might cause discernable changes in the Brownian diffusion and hence require the use of a "limiting breadth" which itself is a function of temperature.

DYNAMICAL COMPUTATION OF PHOTON CORRELATIONS AND COUNTING STATISTICS*†

by

Victor Korenman

Department of Physics and Astronomy
University of Maryland, College Park, Maryland

* Work supported in part by the Air Force Office of Scientic Research under grant no. AF - 735-65; N.A.S.A. grant NGR 21-002-022; and by Advanced Research Projects Agency contract SD-101.

† A preliminary version of this work was presented at the Second Rochester Conference on Coherence and Quantum Optics, June 1966 (unpublished).

ABSTRACT

Equations of motion are derived for generating functions of field correlations and detector counting probabilities for an arbitrary system of electromagnetic fields in the presence of their sources. For a system with linear constitutive relations the equations are solved exactly. Such systems are shown to be always Gaussian and some representative counting distributions are computed. A perturbative treatment of a system with a cubic nonlinearity in its constitutive relation is made to find the counting distribution to first order in the nonlinear coefficient. A comparison is made with the below threshold limit of a recent laser fluctuation theory and a possible application to measurement of phonon-phonon interactions is mentioned.

I. INTRODUCTION

There has recently been a great deal of work, both theoretical[1-3] and experimental[4] on the statistics of photoelectron counting associated with various types of light sources. Counting experiments can serve as a useful diagnostic tool to study the properties of the system in which the light is generated or systems from which it might scatter. There have been two main lines of approach to the calculation of counting statistics. The treatment of thermal or "natural" sources has been essentially kinematical, dealing with the freely propagating electromagnetic fields in a source free region and invoking either a special form for the system's density matrix[2] or an assumption about the "chaotic"[1] nature of the field sources. Calculations concerning lasers[3], on the other hand, have involved detailed dynamical consideration of particular models.

We discuss here a more general dynamical approach, based on techniques which have been useful in Quantum Field Theory and Solid State Physics[5], which should be useful in the analysis of many systems. We write equations of motion for the generating functions of correlations or counting probabilities for an arbitrary system of interacting electromagnetic fields in the presence of their sources (and scatterers), different systems being distinguished according to the form of the field-source interaction. Two cases are treated in some detail. For a system with linear constitutive relations for the electromagnetic field the equations of motion are

exactly integrable and we show that linear systems are always Gaussian, in the sense that all correlation functions are expressible in terms of products of the two point correlation in the usual way[6]. We go on to integrate the equation for the counting probabilities in a linear system in the presence of a prescribed current and find agreement with some previous calculations of Glauber[1D].

The exact integrability of a linear system makes it convenient as a base for a perturbative treatment of a nonlinear system when the deviation from linearity can be considered small. We make such a perturbative expansion of the correlation functions and counting probabilities for a system with a small cubic term in the constitutive equation, to lowest order in the strength of the cubic term. A comparison of the results with the below threshold limit of a previous calculation[7] concerning gas lasers is made, and the possible applicability of this calculation to a proposed experiment[8] on Raman scattering is mentioned.

II. DYNAMICAL APPROACH

To illustrate our approach we first consider equations for a simple generating function of field correlations and show how they are integrated in the linear case. The functional F{j} is defined by[9,10]

$$F\{j\} \equiv \langle (\exp \{ i \sum_{\zeta=+,-} \int_{-\infty}^{\infty} dt d^3r \, \zeta j^{\zeta}(x) \cdot A^{\zeta}(x) \}) _{+} \rangle \qquad (1)$$

where $A(x) \equiv A(rt)$ is the transverse vector potential operator in the Heisenberg picture. The superscripts ζ help to define the operator ordering. Operators with superscript (+) stand to the right in the operator product and are positively time ordered. Operators with ζ = (-) stand to the left and are inversely time ordered. The bracket stands for the usual expectation value. That is

$$\langle 0 \rangle \equiv \mathrm{tr}\, \rho 0 \qquad (2)$$

where ρ is some density matrix characterizing the system. The arbitrary function $j^{\zeta}(x)$ is the argument of our functional F. Field correlation functions are obtained from F{j} through the relations [12]

$$\left(\frac{\delta^{n+m} F\{j\}}{\delta j^{-}(x_1) \ldots \delta j^{-}(x_n) \delta j^{+}(x_1') \ldots \delta j^{+}(x_m')} \right)_{j=0} = i^{m-n} \langle (A(x_1) \ldots A(x_n))_{-}$$

$$(A(x_1') \ldots A(x_m'))_{+} \rangle \qquad (3)$$

Now, following Glauber[1B,C] and Kelley and Kleiner[13] it is easy to show[14] that the n^{th} factorial moment of the photon counting distribution is given by the expression

$$\langle C!/(C-n)!\rangle = \int dx_1 \ldots dx_n dx_1' \ldots dx_n' \prod_{j=1}^{n} g(x_j,x_j') \times$$

$$\times \langle (A(x_1)\ldots A(x_n))_-(A(x_1')\ldots A(x_n'))_+\rangle \qquad (4)$$

$$\text{where } g(rt,r't') = \phi(rt)\,\phi(r't')\delta(r-r') \int_{-\infty}^{\infty} \frac{d\omega}{2\pi} g(r,\omega) e^{-i\omega(t-t')} \qquad (5)$$

The function $\phi(rt)$ is zero or one depending on whether the part of the detector at r is off or on at time t [15] and $g(r\omega)$ is the detector sensitivity at r and frequency ω. Then, comparing (3) with (4) we see that the generating functional $F\{j\}$ generates all the correlation functions of interest in counting experiments. It therefore contains all the information about the system that can be obtained from such experiments.

Now from Maxwell's equations and the electromagnetic field commutation relations we can write

$$\left(\frac{\partial^2}{\partial t^2} - c^2\nabla^2\right) \langle A^\zeta(x)\rangle \equiv \Box \langle A^\zeta(x)\rangle = \langle J^\zeta(x)\rangle + j^\zeta(x) \qquad (6)$$

where

$$\langle A^\zeta(x)\rangle \equiv -i\zeta\, \delta \log F\{j\}/\delta j^\zeta(x) \qquad (7)$$

$$F\{j\}\langle J^\zeta(x)\rangle \equiv \langle (J^\zeta(x) \exp\{i \sum_{\zeta'=-,+} \int_{-\infty}^{\infty} dx'\, \zeta' j^{\zeta'}(x')\cdot A^{\zeta'}(x')\})_+\rangle \qquad (8)$$

and J(x) is the appropriate current operator for the system. As in any discussion of electromagnetism, Maxwell's equations are empty of content until they are supplemented with appropriate constitutive equations. In the present context Eqs. (6) and (7) will be a complete description of the system when the relationship between $\langle J \rangle$ and $\langle A \rangle$ is specified. The nature of this relationship must, of course, be determined through detailed microscopic analysis of the matter-field interaction in any particular case. It is interesting, however, to study the consequences of assumed forms for this relationship.

A type of constitutive relation of particular interest is the linear one, as it is an excellent approximation to the correct relation in the vast majority of physical systems. We define linearity in a somewhat generalized sense as a relation of the form

$$\langle J^{\zeta}(x) \rangle = \sum_{\zeta'} \int dx' \, P^{\zeta\zeta'}(xx') \, \langle A^{\zeta'}(x') \rangle \tag{9}$$

with P not a function of j. We have shown elsewhere[16] that a relation such as (9) implies a field independent incoherent (spontaneous and "thermal") emission rate as well as a linear susceptibility in the usual sense[17].

For such a system Eqs. (6), (7), and (9) may be combined to give

$$[\Box \delta^{\zeta\zeta_1}\delta(x-x_1) - P^{\zeta\zeta_1}(xx_1)] \left(\frac{-i\zeta_1 \delta \log F\{j\}}{\delta j^{\zeta_1}(x_1)} \right) = j^{\zeta}(x)^{18} \tag{10}$$

which may be immediately integrated as

$$F\{j\} = \exp\left[\frac{i}{2}\ \zeta j^{\zeta}(x)\ D^{\zeta\zeta'}(xx')j^{\zeta'}(x')\right] \tag{11}$$

where D satisfies

$$[\Box\delta^{\zeta\zeta_1}\delta(x-x_1)-P^{\zeta\zeta_1}(xx_1)]\ D^{\zeta_1\zeta'}(x_1x') = \delta^{\zeta\zeta'}\delta(x-x').^{19} \tag{12}$$

From Eqs. (3) and (11) we see immediately that D is the two point correlation function and Eq. (11) shows that a linear system is always "Gaussian" no matter what form the two point correlation may take[20,21]. A similar result has been established by Glauber[1B] for "chaotic" field sources. It may be that linearity and chaoticity are complementary descriptions of the same physical situation. The criterion of linearity, however, is perhaps more precise.

For the sake of completeness and for use in the sequel let us complete our analysis of Eq. (10) for F{j} by seeing what information is contained in Eq. (12) for D. Comparing Eq. (3) with Eq. (11) it is easy to show that the $\zeta\zeta'$ structure of $D^{\zeta\zeta'}(xx')$ can be expressed in the matrix form

$$D^{\zeta\zeta'}(xx') = d^{r}(xx')\begin{pmatrix}1 & 0\\ 0 & 1\end{pmatrix} + \begin{pmatrix}d^{<}(xx') & -d^{<}(xx')\\ d^{>}(xx') & -d^{>}(xx')\end{pmatrix} \tag{13}$$

where

$$d^{>}(xx') = d^{<}(x'x) \equiv i\ (\langle A(x)A(x')\rangle - \langle A(x)\rangle\langle A(x')\rangle) \tag{14a}$$

$$d^{r}(xx') = d^{a}(x'x) \equiv \eta(t-t')\ [d^{>}(xx')-d^{<}(x'x)] \tag{14b}$$

and $\eta(t)$ is unity for t positive and zero otherwise. Then, as we have shown elsewhere[22], Eq. (12) can be easily decomposed into the two equations

$$[\Box\delta(x-x_1)-p^r(xx_1)]d^r(x_1x') = \delta(x-x') \tag{15a}$$

$$[\Box\delta(x-x_1)-p^r(xx_1)]d^<(x_1x') = p^<(x\,x_1)d^a(x_1x') \tag{15b}$$

where p^r and $p^<$ are elements of $P^{\zeta\zeta'}$ in a decomposition identical to Eq. (13). Now Eq. (15a) is the equation for the classical Green's function of the electromagnetic field in a region of (frequency, wavenumber, time, and position dependent) linear susceptibilities. As in the classical case this equation determines the mode or quasimode structure of the region as well as the frequency spectrum in terms of the (complex) susceptibility p^r.

From (14a) we see that $d^<$ contains the energy density (power spectrum) of the field as d^r does not. Equation (15b) which determines this quantity is conveniently written in the integrated form

$$d^<(xx') = d^r(xx_1)p^<(x_1x_2)d^a(x_2x') \tag{16}$$

which has been shown elsewhere[11] to determine the energy density by detailed balance of incoherent emission into the system, described by $p^<$, and absorptive losses contained in the Green's functions d^r and d^a. We note that thermal equilibrium would imply a relationship (fluctuation dissipation theorem) between p^r and $p^<$ which is just of

the correct form to ensure that $d^{<}(xx')$ embodies the Planck distribution in that case.

Then we have completely solved the general equations (6) and (7) for all the physically relevant correlation functions of the electromagnetic field in a medium with linear constitutive equations, in terms of the susceptibility and spontaneous emission rate which characterize the medium completely. We could, at this point, either go on to consider these equations for nonlinear media or show how counting distributions for linear systems are obtainable from the above results[23]. It is more convenient, however, for both these discussions first to introduce a more general generating functional and discuss its equations of motion. In the next section we introduce this new functional and go on to compute the linear system counting distribution.

III. IMPROVED GENERATING FUNCTIONAL AND LINEAR COUNTING DISTRIBUTION

We define a new generating functional $F'\{j,U\}$ by

$$F'\{j,U\} \equiv \langle(\exp i[\zeta j^{\zeta}(x)\cdot A^{\zeta}(x)+A^{\zeta}(x)U^{\zeta\zeta'}(xx')A^{\zeta'}(x')])_{+}\rangle \qquad (17)$$

where now both j and U are independent variables[18]. Comparing Eq. (1) we see that $F'\{j,U=0\} = F\{j\}$. The particular utility of F', however, is seen by noting that, in view of Eq. (4)

$$F'\{j=0,U^{\zeta\zeta'}(xx') = \lambda\delta^{\zeta,-}\delta^{\zeta',+}g(xx')\} = \sum_{n=0}^{\infty}\frac{(i\lambda)^n}{n!}\langle C!/(C-n)!\rangle \qquad (18)$$

so that F' contains an explicit generating function for factorial moments of the counting distribution[24]. Using the relation from Glauber[16] or Kelley and Kleiner[13]

$$\sum_{n=0}^{\infty}\frac{(i\lambda)^n}{n!}\langle C!/(C-n)!\rangle = \sum_{m=0}^{\infty}(1+i\lambda)^m p_m \qquad (19)$$

where p_m is the probability of m counts, we see that F' generates the counting distribution itself as well. Finally, as is evident from Eq. (6) for $F\{j\}$ and the equations below for $F'\{j,U\}$, $j^{\zeta}(x)$ plays the role of a prescribed current driving the system. Then $F'\{j,U\}$ with the value for U used in Eq. (18) and $j^{+}(x)=j^{-}(x) \equiv j(x)$ chosen appropriately is a generating function for the counting distribution for the system of interest in the presence of a prescribed driving current. Such an expression, when it can be evaluated, might describe the statistics of the scattered light from

• medium illuminated, say, by a highly coherent laser source[26]. A prescribed current in a linear system has also been a useful model in discussing laser fluctuations[1D].

Now corresponding to Eqs. (6) and (7) for $F\{j\}$, $F'\{j,U\}$ satisfies

$$[\Box\,\delta^{\zeta\zeta_1}(x-x_1)-\tilde{U}^{\zeta\zeta_1}(xx_1)]\left(\frac{-i\zeta_1\delta\log F'\{j,U\}}{\delta j^{\zeta_1}(x_1)}\right)=\langle J^{\zeta}(x)\rangle+j^{\zeta}(x) \tag{20}$$

where

$$\tilde{U}^{\zeta\zeta_1}(xx_1) \equiv \zeta[U^{\zeta\zeta_1}(xx_1)+U^{\zeta_1\zeta}(x_1x)] \tag{21}$$

while the identities

$$\frac{\delta^2\log F'\{j,U\}}{\delta j^{\zeta}(x)\delta j^{\zeta'}(x')} \equiv i\zeta D^{\zeta\zeta'}(xx') = i\zeta' D^{\zeta'\zeta}(x'x) = i\zeta\delta\langle A^{\zeta}(x)\rangle/\delta j^{\zeta'}(x')$$

$$= i\zeta\zeta'\left[\frac{\delta\log F'\{j,U\}}{\delta U^{\zeta\zeta'}(xx')} - \langle A^{\zeta}(x)\rangle\langle A^{\zeta'}(x')\rangle\right] \tag{22}$$

allow us to write the result of differentiating Eq. (20) with respect to $j^{\zeta'}(x')$ as

$$[\Box\,\delta^{\zeta\zeta_1}(x-x_1)-\tilde{U}^{\zeta\zeta_1}(xx_1)]\left[\frac{\zeta'\delta\log F'\{j,U\}}{\delta U^{\zeta_1\zeta'}(x_1x')} - \zeta'\langle A^{\zeta_1}(x_1)\rangle\langle A^{\zeta'}(x')\rangle\right]$$

$$= \frac{\delta\langle J^{\zeta}(x)\rangle}{\delta j^{\zeta'}(x')} + \delta^{\zeta\zeta'}(x-x').^{27} \tag{23}$$

Equations (20)-(23) again form a complete description of the system in question as soon as a constitutive equation relating

<J> to <A> is specified.

For a linear system the integration of these equations is again straightforward. Thus Eq. (20) with Eq. (9) can be integrated just as Eq. (10) to give

$$F'\{j,U\} = F'\{j=0,U\}\ \exp\tfrac{i}{2}[\zeta j^{\zeta}(x)D^{\zeta\zeta'}(xx';U)j^{\zeta'}(x')] \tag{24}$$

where D(U) is defined by

$$[\Box\,\delta^{\zeta\zeta_1}(x-x_1)-P^{\zeta\zeta_1}(xx_1)-\tilde{U}{}^{\zeta\zeta_1}(xx_1)]D^{\zeta_1\zeta'}(x_1x';U) = \delta^{\zeta\zeta'}(x-x') \tag{25}$$

Then, noting that <A> = 0 when j = 0, Eq. (23), with Eqs. (9) and (22) is

$$[\Box\ -P-\tilde{U}]^{\zeta\zeta_1}(xx_1)\ \frac{\zeta'\delta\log F'\{0,U\}}{\delta U^{\zeta_1\zeta'}(x_1x')} = \delta^{\zeta\zeta'}(x-x') \tag{26}$$

where an obvious shorthand has been employed. Now taking account of the symmetry of the problem under matrix transposition of U we may write (26) as

$$\delta\log F'\{0,U\} = \tfrac{1}{2}\,(\Box\ -P-\tilde{U})^{-1}\ {}^{\zeta\zeta_1}(xx_1)\ \delta\tilde{U}{}^{\zeta_1\zeta}(x_1x)$$

$$= \tfrac{1}{2}\ \mathrm{tr}\ [(1-D_o\tilde{U})^{-1}\ \delta(D_o\tilde{U})] \tag{27}$$

where

$$D_o = (\Box\ -P)^{-1} = D(U=0) \tag{28}$$

and we have gone over to a full matrix notation. We recognize Eq. (27) as being equivalent to

$$\delta \log F'\{0,U\} = -\frac{1}{2}\,\delta\ \mathrm{tr}\ \log(1-D_o\tilde{U}) \tag{29}$$

so that, with Eq. (24) we have the exact solution

$$F'\{j,U\} = \exp\frac{i}{2}\,\mathrm{tr}\{(1-D_o\tilde{U})^{-1}D_o jj\zeta + i\log(1-D_o\tilde{U})\}. \tag{30}$$

Note that this is still, in principle, completely determined by the system susceptibilities $p^<$ and p^r since, by Eq. (28), D_o is the same as D of the previous section and determined by Eqs.(15).

Let us now see how a photocount distribution can be extracted from Eq. (30). We choose the form of U as in Eq. (18) and expand F' as

$$F'\{j,\lambda g\} \equiv \exp\{\sum_{n=0}^{\infty} \lambda^n K_n\} \tag{31}$$

where K_n is explicitly evaluated by expanding Eq. (30) as

$$\lambda^n K_n = \frac{i}{2}\,[j^{\zeta_1}(x_1)\zeta_1 D_o^{\zeta_1\zeta_2}(x_1x_2)\tilde{U}^{\zeta_2\zeta_3}(x_2x_3)D_o^{\zeta_3\zeta_4}(x_3x_4)\cdots$$

$$\cdots\ \tilde{U}^{\zeta_{2n},\zeta_{2n+1}}(x_{2n}x_{2n+1})D_o^{\zeta_{2n+1}\zeta_{2n+2}}(x_{2n+1}x_{2n+2})j^{\zeta_{2n+2}}(x_{2n+2})]$$

$$+\frac{1}{2n}\,[D_o^{\zeta_1\zeta_2}(x_1x_2)\cdots\tilde{U}^{\zeta_{2n},\zeta_1}(x_{2n},x_1)] \tag{32}$$

and we still use the convention of summing over repeated indices ζ and integrating over repeated variables x.

Now by inverting Eq. (10) and remembering the definition Eq. (28) of D_o it is easy to see that

$$D_o^{\zeta\zeta'}(xx')j^{\zeta'}(x') = \langle A^{\zeta}(x)\rangle, \tag{33}$$

that is, the coherent field generated by the prescribed current. Then the two j's in the first term of Eq. (32) and their adjacent D_o's can be written using the symmetry relation (22) as

$$\zeta_2\langle A^{\zeta_2}(x_2)\rangle\langle A^{\zeta_{2n+1}}(x_{2n+1})\rangle = -iD_c^{\zeta_{2n+1},\zeta_2}(x_{2n+1},x_2) \tag{34}$$

and we may rewrite Eq. (32) as

$$\lambda^n K_n = \frac{1}{2n}\left[(D(12)+nDc(12))\tilde{U}(23)D(34)\tilde{U}(45)....D(2n-1,2n)\tilde{U}(2n,1)\right] \tag{35}$$

where now (1) is shorthand for (x_1,ζ_1).

Equation (35) can be further simplified if the detector system has certain properties. Let us more closely examine a portion of the product above. Thus

$$\lambda^{-2}\tilde{U}(23)D_o(34)\tilde{U}(45) = \int_{-\infty}^{\infty} dt_3 dt_4 \frac{d\omega_1 d\omega_2 d\Omega d\omega_3}{(2\pi)^4} \quad x$$

$$x\ \ \phi(r_2t_2)[-\delta^{\zeta_2,-}\delta^{\zeta_3,+}g(r_2\omega_1)+\delta^{\zeta_2,+}\delta^{\zeta_3,-}g(r_2,-\omega_1)]\phi(r_2t_3)D_o^{\zeta_3\zeta_4}(r_2r_5,\omega_2\Omega)$$

$$x\ \ \phi(r_5t_4)[-\delta^{\zeta_4,-}\delta^{\zeta_5,+}g(r_5\omega_3)+\delta^{\zeta_4,+}\delta^{\zeta_5,-}g(r_5,-\omega_3)]\phi(r_5t_5)$$

$$x\ \ \exp -i[\omega_1(t_2-t_3)+\omega_2(t_3-t_4)+\tfrac{1}{2}\Omega(t_3+t_4)+\omega_3(t_4-t_5)] \tag{36}$$

where we have used Eqs. (5), (18), and (21) and the Ω dependence of D reflects a possible nonstationarity of the system. The simplification

mentioned above obtains if we may say either that the detector only operates on transitions to a higher energy state, so that $g(\omega)$ is nonzero only at positive optical frequencies[28], or that it operates on transitions to a lower state[29] so that only negative ω contribute. Then, considering that Ω is small relative to optical frequencies and that $\phi(t)$ defines an interval long compared to inverse optical frequencies, the t_3 and t_4 integrals in Eq. (36) ensure that $\omega_1 \approx \omega_2 \approx \omega_3$ where the $\approx$ sign means close compared to optical frequencies. But since $g(\omega)g(-\omega') = 0$ when $\omega \approx \omega'$ the only terms surviving of the four in Eq. (36) are those coupling $g(\omega_1)$ with $g(\omega_3)$ and $g(-\omega_1)$ with $g(-\omega_3)$. That is, reconstructing the Fourier transforms,

$$\lambda^{-2}\tilde{U}(23)D_o(34)\tilde{U}(45) = \delta^{\zeta_{2,-}}g(x_2x_3)D_o^{+-}(x_3x_4)g(x_4x_5)\delta^{\zeta_{5,+}}$$

$$+\delta^{\zeta_{2,+}}g(x_3x_2)D_o^{-+}(x_3x_4)g(x_5x_4)\delta^{\zeta_{5,-}} . \qquad (37)$$

Extending this argument to the full expression (35) it is easily shown that K_n is the sum of two terms, one containing D_o^{+-} and g in the correct matrix order while the other involves D_o^{-+} and g in transposed order. Finally, exploiting the symmetries inherent in Eqs. (13) and (14) one easily shows that the two terms are equal so that K_n is finally written

$$K_n = \frac{1}{n}\left[(d^<(x_1x_2)+nd_c^<(x_1x_2))g(x_2x_3)d^<(x_3x_4)\ldots g(x_{2n},x_1)\right] \qquad (38)$$

and F' may be reconstructed as

$$F'\{j,\lambda g\} = \exp \mathrm{tr}\,[\lambda d^{<}_{c}\, g\,(1-\lambda d^{<} g)^{-1} - \log\,(1-\lambda d^{<} g)]. \quad (39)$$ [30]

Equations (38) and (39) are now in a form which is easily treated in certain, physically relevant, special cases. Thus, with a thin detector oriented normally to a well collimated beam and a counting time short compared to the coherence time in $d^{<}$, one finds in the usual way[1C]

$$F'\{j,\lambda g\} = \frac{1}{1-i\lambda\langle C\rangle} \exp\left(\frac{i\lambda\langle C\rangle_c}{1-i\lambda\langle C\rangle}\right) \quad (40)$$

where

$$i\langle C\rangle \cong \bar{g}T\sum_k \int_0^\infty \frac{d\omega}{2\pi} \int_{-\infty}^{\infty} \frac{d\Omega}{2\pi}\, d^{<}_{k}(\omega,\Omega) \quad (41a)$$

$$\langle C\rangle_c \cong \bar{g} \int d^3r \int_0^\infty \frac{d\omega}{2\pi} \left| \int_{-\infty}^{\infty} dt\, \phi(rt)\langle A(rt)\rangle e^{i\omega t} \right|^2 \quad (41b)$$

and $\bar{g}$ is a suitable average counter sensitivity. Equation (40) is identical to one obtained by Glauber[1D] for this case via a quite different route. The opposite case of a long counting interval yields the result

$$F'\{j,\lambda g\} = \exp\left\{\frac{1}{2}T\zeta\left[1-\left(1-\frac{4i\lambda\langle C\rangle}{T\zeta}\right)^{1/2}\right] + \frac{i\lambda\langle C\rangle_c}{1-\frac{i\lambda\langle C\rangle}{T\zeta}\;\frac{\zeta^2}{\Delta^2+\frac{1}{4}\zeta^2}}\right\} \quad (42)$$

where we have assumed a Lorentzian spectrum of full width ζ and Δ is the difference between the center frequency of the Lorentzian

line and the assumed single frequency of the coherent signal. The factorial moments and counting distributions corresponding to Eqs. (40) and (42) are found by use of Eqs. (18) and (19).

IV. SOME NONLINEAR RESULTS

In addition to the exact results (eg. Eq. (30) or (39)) we have obtained for linear systems it is possible to extract from the equations ((20)-(23)) for $F'\{j,U\}$ some approximate results for nonlinear systems. For example, if the constitutive equation includes a cubic term

$$\langle J^{\zeta}(x)\rangle = P^{\zeta\zeta_1}(xx_1)\langle A^{\zeta_1}(x_1)\rangle - i\zeta\, \Gamma^{\zeta\zeta_1\zeta_2\zeta_3}(xx_1x_2x_3)\langle A^{\zeta_1}(x_1)A^{\zeta_2}(x_2)A^{\zeta_3}(x_3)\rangle \tag{43}$$

then Eq. (23) for $F'\{j,U\}$ (in the $j = 0$ limit) can be written

$$\left\{\Box\,\delta(1-\bar{1}) - P(1\bar{1}) - \tilde{U}(1\bar{1}) + \zeta\Gamma(1\bar{1}23)\left[\frac{\delta}{\delta U(23)} + D(23)\zeta_3\right]\right\}D(\bar{1}1') = \delta(1-1'), \tag{44}$$

and the expression (Eq. (22)) for D as a derivative of F' makes a complete closed set of equations for F'. The constitutive equation (43), with a particular evaluation of Γ has been the basis for a number of laser theories[11,31]. It may also be appropriate for the description of anharmonic phonons in some materials.

We treat here only the deviations from Gaussian behavior induced by the cubic term in Eq. (43) to lowest order in the nonlinear coefficient function Γ. For clarity we leave the details of the perturbation scheme to an appendix and just note the basic result for the correlation function

$$G(1,\ldots,2n) \equiv \langle A(1)\ldots A(2n)\rangle \quad [32]$$

$$= \sum_M D'(j_1 j_2) D'(j_3 j_4)\ldots D'(j_{2n-1}\, j_{2n})$$

$$- \sum_M L(j_1 j_2 j_3 j_4) D'(j_5 j_6)\ldots D'(j_{2n-1}\, j_{2n}) \qquad (45)$$

where $\sum_M$ means the sum over all maps of $1,\ldots,2n$ onto $j_1,\ldots,j_{2n}$ except that maps which differ only by a permutation of indices inside a D' or L are considered to be the same. D'(12) is the symmetric two point function $D^{\zeta_1\zeta_2}(x_1x_2)\zeta_2 = i\langle A^{\zeta_1}(x_1)A^{\zeta_2}(x_2)\rangle$ while L(1234) is the fully symmetric expression

$$L(1234) \equiv D'(1\bar{1})D'(2\bar{2})\{\Gamma(\bar{1}\bar{2}\bar{3}\bar{4})+\Gamma(\bar{1}\bar{2}\bar{4}\bar{3})+\Gamma(\bar{1}\bar{3}\bar{2}\bar{4})+\Gamma(\bar{1}\bar{3}\bar{4}\bar{2})$$
$$+ \Gamma(\bar{1}\bar{4}\bar{2}\bar{3})+\Gamma(\bar{1}\bar{4}\bar{3}\bar{2})\}D'(\bar{3}\bar{3})D'(\bar{4}\bar{4}) \qquad (46)$$

which describes the interaction of a single pair of photons via the nonlinearity.

In the same approximation D satisfies the equation (when U is finally set to zero)

$$\{\Box\,\delta(1-\bar{1})-P(1\bar{1})+\zeta[\Gamma(1\bar{1}23)+\Gamma(12\bar{1}3)+\Gamma(123\bar{1})]D'(23)\}D(\bar{1}1') = \delta(1-1') \qquad (47)$$

which gives the first order effects of the nonlinearity on the mode structure, spectrum and power spectrum of the system.[33]

Now the particular part of G which is measured by an absorptive detector is

$$G'(1',\ldots n';\ 1,\ldots n) \equiv \langle A^-(1')\ldots A^-(n')A^+(1)\ldots A^+(n)\rangle \qquad (48)$$

where, in addition to the ordering implied by the choice of superscripts, A(1)...A(n) have only their positive frequency parts contributing while A(1')...A(n') contribute with negative frequency only. The terms of Eq. (45) which survive in G' are

$$G'(1',\ldots n';1,\ldots n) = \sum_M d^<(1,j_1)d^<(2,j_2)\ldots d^<(n,j_n)$$

$$- \sum_\pi \sum_M{}' L^{++--}(\ell,m,j_\ell,j_m)[d^<(1,j_1)\ldots d^<(n,j_n)]' \qquad (49)$$

where $\sum_M$ means the sum over the n! maps of $1',\ldots n'$ into $j_1,\ldots,j_n$, $\sum_M'$ does not distinguish maps which differ only by exchanging j_ℓ and j_m, $\sum_\pi$ means we sum as well over partitions which choose the variables in L and the prime on the product in the L dependent term means that there are only n-2 factors as the variables which appear in L do not appear in the product. There are $\frac{1}{4}n(n-1)n!$ terms in the second sum. Finally we have used Eq. (13) to write D'^{+-} as $d^<$.

With Eq. (4), Eq. (49) again predicts counting distributions. In the limit of short counting times compared to the coherence times in D and Γ and for the simple field and detector geometry we have previously used, one finds, for example, the factorial moments

$$< C!/(C-n)!> = n!<C>^n[1- \tfrac{1}{4}n\ (n-1)L] \qquad (50)$$

where <C> is defined in Eq. (41a) and L is the value of L(1234) with all times set equal, divided by the square of the field intensity. Then, using Eq. (19) we find for the probability of

m counts[34]

$$P_m = \frac{1}{1+\langle C\rangle}\left(\frac{\langle C\rangle}{1+\langle C\rangle}\right)^m \left\{1-\frac{1}{4}L\left[2-\frac{4(m+1)}{\langle C\rangle+1}+\frac{(m+1)(m+2)}{(\langle C\rangle+1)^2}\right]\right\}. \qquad (51)$$

Although Eqs. (45)-(51) contain only the simplest effects of the nonlinearity on the system in question the results are still of some physical interest. Let us briefly mention several points.

In the first place, Eqs. (50) and (51) show that, no matter how weak the interaction strength L, correlation functions of sufficiently high order are strongly modified to first order in the nonlinearity. While it is possible that higher order terms in Γ would change this conclusion, yet it strongly suggests that, since there is a small photon-photon interaction even in the vacuum, it is never correct to think of a photon field as linear (or Gaussian) to a good approximation if correlation functions of all orders are being considered.

Secondly, as mentioned above, Eq. (43) can describe a laser, and our result Eq. (51) for a counting distribution should be valid in a region of operation (below threshold) where the nonlinear effects are still weak. An evaluation of L and an analysis of Eq. (47) for the linewidth and intensity of Lamb's gas laser model has been carried out in this region, using the evaluation of Γ from Ref. (11). The results are as follows.

The parameter L in Eq. (51) can be expressed as $L = \rho^2 N^2$, where N is the number of photons in the mode, (defined as the average energy in the mode divided by $h\nu$) while the constant ρ characterized the laser in question and is evaluated as

$$\rho^2 \equiv \frac{\lambda^3}{8\pi V} \frac{\gamma_2'}{\gamma_2} \frac{\omega_o}{\gamma_1} . \qquad (52)$$

Here λ and ω_o are the wavelength and circular frequency of the laser line, V is the "mode volume", which should be taken as the physical volume of the beam, γ_2 and γ_1 are the natural linewidths of the upper and lower levels respectively and γ_2' is that part of the upper level natural linewidth due to transitions to level one. A typical value for ρ in a gas laser might be 10^{-4}. In this same approximation the intensity satisfies the relation

$$\rho N = \frac{1}{2} w + \sqrt{\frac{1}{4}w^2+1} \qquad (53)$$

where

$$w = \frac{1}{\rho} \frac{n-1}{n} \qquad (54)$$

and n is the ratio of the level inversion to that required for the nominal threshold[35]. The linewdith satisfies the Townes relation[36].

The above results have been compared to those of Risken[37], which are valid for all intensities. In the limit of small intensity the counting distribution derived from Risken's intensity distribution reduces exactly to the form of Eq. (51). Furthermore a comparison with his expression for the average intensity shows that L is evaluated identically and that his w and our w are the same parameter. Then Eq. (54) may be taken as an evaluation of Risken's excitation parameter in terms of the physical constants of a gas laser system.

As a final application of Eq. (51) (or the corresponding results for similar constitutive relations) let us consider a recent

proposal[8] for using intensity correlations in Raman scattering to measure the lifetimes of optical phonons in crystals. Briefly, Fetter shows that the correlation functions of the scattered light, when the incoming light is coherent, are directly related to phonon correlation functions in the crystal, with the same ordering as the correlation functions we have been discussing[38]. Then the deviation of the counting statistics of the scattered light from Gaussian will reflect a nonlinearity in the phonon system and may allow an estimate of the strength of the phonon-phonon interaction in the crystal. The feasibility of an experiment along these lines is being examined.

V. CONCLUSION

In summary then, we have derived dynamical equations for generating functionals of the physically interesting correlation functions of any system of interacting photons in the presence of their sources. We have shown that for the important subclass of linear systems the equations are exactly integrable, and that these systems always have Gaussian behavior, whether or not they are stationary and independent of the spectrum and power spectrum. An explicit expression from which counting probabilities are obtainable was developed and was evaluated for some physically interesting cases of simple source and detector characteristics.

We then treated a system with a cubic nonlinearity in the constitutive equation, by perturbation theory, to lowest order in the nonlinear coefficient. From the expression for the counting probabilities we conclude that any small nonlinearity spoils the Gaussian behavior for a sufficiently high order correlation function. The results are in agreement with the appropriate limit of a nonlinear laser theory developed by Risken, and a possible application to the measurement of phonon-phonon interactions in a crystal is discussed.

APPENDIX

NONLINEAR PERTURBATION THEORY

We sketch the steps leading from Eq. (44) in Section IV to Eqs. (45)-(47). First, noting that the relation $D^{-1}(1\bar{1})D(\bar{1}2') = \delta(1-2')$ implies

$$\frac{\delta D(12)}{\delta U(34)} = -D(1\bar{1}) \frac{\delta D^{-1}(\bar{1}\bar{2})}{\delta U(34)} D(\bar{2}2) \tag{55}$$

we rewrite Eq. (44) as

$$\left\{\square\delta(1-\bar{1})-P(1\bar{1})-\tilde{U}(1\bar{1})+\zeta\Gamma(1423)\left[D'(23)\delta(4-\bar{1})-D(45)\frac{\delta D^{-1}(5\bar{1})}{\delta U(23)}\right]\right\}$$

$$\times \quad D(\bar{1}1') = \delta(1-1') \tag{56}$$

which identifies the quantity in curly brackets as $D^{-1}(1\bar{1})$ and provides an exact equation for this quantity. An iterative solution to this equation in powers of Γ is easily obtained, of which we retain only the first term

$$D^{-1}(1\bar{1}) \approx \square\,\delta(1-\bar{1})-P(1\bar{1})-\tilde{U}(1\bar{1})+\zeta\tilde{\Gamma}(1\bar{1}23)D'(23) \tag{57}$$

where we define

$$\tilde{\Gamma}(1\bar{1}23) = \Gamma(1\bar{1}23)+\Gamma(12\bar{1}3)+\Gamma(123\bar{1}). \tag{58}$$

Equations (57) and (58) immediately yield Eq. (47). Equation (45) is obtained by noting that

$$G(1,\ldots,2n) = (-i)^n \left(\frac{\delta}{\delta U(12)} + D'(12)\right)\left(\frac{\delta}{\delta U(34)} + D'(34)\right) \times$$

$$\times \ldots \left(\frac{\delta}{\delta U(2n-3,2n-2)} + D'(2n-3,2n-2)\right) \times D'(2n-1,2n) \qquad (59)$$

which follows from Eqs. (17) and (22) when j = 0. Thus

$$G(1234) = -D'(12)D'(34) + D(35)\frac{\delta D^{-1}(56)}{\delta U(12)} D'(64) \qquad (60)$$

which is, to lowest order, according to Eqs. (57) and (21)

$$\begin{aligned} -G(1234) &\approx D'(12)D'(34)+D'(13)D'(24)+D'(14)D'(23) \\ &\quad - D'(35)\tilde{\Gamma}(5678)\frac{\delta D'(78)}{\delta U(12)} D'(64) \\ &\approx D'(12)D'(34)+D'(13)D'(24)+D'(14)D'(23)-L(1234) \end{aligned} \qquad (61)$$

where the last step again involves taking the lowest order term and L is defined in Eq. (46). It is easy to show that repeated use of this procedure enables one to write Eq. (59) as Eq. (45) to lowest order in Γ.

FOOTNOTES

1. A. R. J. Glauber, Phys. Rev. Letters 10, 84 (1963)

   B. Phys. Rev. 131, 2766 (1963)

   C. Quantum Optics and Electronics, Les Houches 1964 (Gordon and Breach, New York, 1965).

   D. Physics of Quantum Electronics, P. L. Kelley, B. Lax and P. E. Tannenwald, eds., (McGraw-Hill, New York, 1966).

2. C. L. Mehta and E. Wolf, Phys. Rev. 134, A1143, A1149 (1964), L. Mandel and E. Wolf, Rev. Mod. Phys. 37, 231 (1965), E. F. Keller, Phys. Rev. 139, B202 (1965)

3. M. Scully and W. E. Lamb, Jr., Phys. Rev. Letters 16, 853 (1966) H. Risken, Z. Physik 186, 85 (1965); M. Lax and R. D. Hempstead, to be published.

4. C. Freed and H. A. Haus, Phys. Rev. Letters 15, 943 (1965); J. A. Armstrong and A. W. Smith, Phys. Rev. 140, A155 (1965), Phys. Rev. Letters 16, 1169 (1966); F. A. Johnson, T. P. McLean and E. R. Pike, Physics of Quantum Electronics, P. L. Kelley, B. Lax and P. E. Tannenwald, eds., (McGraw-Hill, New York, 1966); F. T. Arecchi, Phys. Rev. Letters 15, 912 (1965); F. T. Arecchi, A. Berne and P. Bulamacchi, Phys. Rev. Letters 16, 32 (1966); W. Martienssen and E. Spiller, Phys. Rev. Letters 16, 531 (1966), Phys. Rev. 145, 285 (1966).

5. See, for example, P. C. Martin and J. Schwinger, Phys. Rev. 115, 1342 (1959); A. A. Abrikosov, L. P. Gor'kov and I. Ye Dzyaloshinskii, Methods of Quantum Field Theory in Statistical Physics (Prentice-Hall, 1963). L. P. Kadanoff and G. Baym, Quantum Statistical Mechanics (W. A. Benjamin, New York, 1962).

6. The general 2n point correlation function has $2^{-n}(2n)!/n!$ terms, one for each different partition of the 2n indices into sets of two.

7. H. Risken, Ref. 3.

8. A. L. Fetter, Phys. Rev. 139, A1616 (1965)

9. F{j} is very similar to a generating functional used by Glauber (Ref. 1C, Eq. 14, 23). Note, however, that we do not take positive and negative frequency parts. For interacting fields the positive and negative frequency parts do not satisfy simple commutation relations nor simple equations of motion.

10. Such generating functionals were introduced by J. Schwinger, J. Math. Phys. 2, 407 (1961). They are particularly suited to the discussion of nonequilibrium systems and were used in a discussion of lasers by the author. (See ref. 11.)

11. V. Korenman, Annals of Physics, N.Y. 39, 72 (1966); Physics of Quantum Electronics, P. L. Kelley, B. Lax and P. E. Tannenwald, eds. (McGraw-Hill, New York, 1966).

12. See Lecture XIV of Ref. 1C for a discussion of functional differentiation.

13. P. L. Kelley and W. H. Kleiner, Phys. Rev. 136, A316 (1964).

14. In particular we follow Glauber's discussion in Ref. (1C) Lectures IV and V except that we retain the ordering of the (now interacting) electromagnetic field operators, do not separate into positive and negative frequency parts and allow the detector to be in any initial ensemble of states. The use of the vector potential A instead of the electric field E just corresponds to a factor of the frequency squared in the definition of the detector sensitivity function. The connection of the calculation in Lecture V of Ref. (1C) with factorial moments is made in Lecture XVII. Note that for the usual counters considered $g(r\omega)$ only contains positive or negative optical frequencies, and the time integrations in Eq. (4) extract the expected frequency parts from the A(x). For radically different types of detectors Eq. (4) may be modified but we still expect the electromagnetic field operators to come in with the same type of ordering.

15. For a single detector $\phi(rt)$ will be independent of r. The general form is useful in describing multicounter delayed correlation experiments.

16. Ref. (11). Also see below.

17. In thermal equilibrium the susceptibility and incoherent emission rate are related by the fluctuation-dissipation theorem and either of the two properties mentioned here implies the other. This is no longer the case when thermal equilibrium does not hold.

18. Here and henceforth we use the convention of summing over repeated indices and integrating over repeated variables.

19. To get from Eq. (10) to Eq. (11) we have implicitly assumed the symmetry of $D^{\zeta\zeta'}(xx')\zeta'$ and thus of $P^{\zeta\zeta'}(xx')$. But the symmetric function $\delta\langle A^{\zeta}(x)\rangle/\delta j^{\zeta'}(x')$ also satisfies Eq. (12) so we must choose P with the required symmetry for a physically realizable system.

20. This is a little different from a classical Gaussian system as the correlation functions refer to operators which do not commute. Only the physical operator orderings (Eq. (3)) are included and the order is retained in the decomposition in terms of two point functions where relevant, that is, within any single two point function.

21. One caveat is necessary. Equation (11) might seem to imply that every field once escaped from its generating region and in the linear region of free space becomes Gaussian. This is clearly not the case and the difficulty arises because we have ignored initial conditions in integrating Eq. (10). Equation (11) then does not apply to free fields, where the initial conditions are always important, and applies to interacting fields only insofar as the interaction has been linear for a time long compared with the relaxation time (inverse bandwidth) contained in D so that initial correlations have damped out and the field is determined by its linear sources.

22. Ref. (11), footnote (10).

23. Counting distributions are found this way in Ref. (1C).

24. For this choice of U, F' is Glaubers $Q(\lambda)$, defined in Ref. (1C), Lecture XVII.

25. For a real prescribed external source $j^{+} = j^{-}$ so that in Eq. (10) the physically required relation $\langle A^{+}\rangle = \langle A^{-}\rangle$ holds.

26. The prescribed current here would be an effective current chosen to mimic the active laser region.

27. Corresponding to the transverse nature of the electromagnetic field the δ function in Eq. (23) should be a transverse δ function. This will be irrelevant in what follows and we henceforth ignore it.

28. See Eqs. (4) and (5) and Ref. (1C) Lecture IV.

29. Such "stimulated emission" detectors have been analyzed by L. Mandel, Bull. Am. Phys. Soc. 11, 111 (1966).

30. Compare Ref. (1C), Eq. 17.45. The difference between absorption and emission detectors is easily seen from Eqs. (38) and (39). Thus if only positive ω appear in g, only $d^{<}(\omega)$, $\omega > 0$, appears in F'. From its' definition in Eq. (14) this is essentially Glaubers $i\langle b^{\dagger}b\rangle$, the photon density. For a stimulated emission counter $d^{<}(-\omega) = d^{>}(\omega) \approx i\langle bb^{\dagger}\rangle$ enters, which is the photon number plus one.

31. W. E. Lamb, Jr., Phys. Rev. 134, A1429 (1964); H. Haken and H. Sauermann, Z. Physik 173, 261 (1963) 176, 47 (1963).

32. The variable (1) still means (x_1,ζ_1) and these correlation functions are the ordered ones defined in Section II.

33. A decomposition such as Eq. (15) still holds with p^{r} and $p^{<}$ now including $\Gamma D'$ terms. Then Eq. (15a) gives the Green's function for a nonlinear dielectric and Eqs. (15b) and (16) describe an intensity dependent incoherent emission rate, arising, for example, from depletion of an upper level due to stimulated emission driven by the local intensity.

34. The first term in Eq. (51) is the well known result for a Gaussian system. See, for example, Ref. (1C).

35. We emphasize that these equations can be taken seriously only for values of ρN small compared to unity, or $\bar{w} \approx -5$ or less. The smallness of ρ and Eq. (54), however, still allow this to be very close to the threshold value of pumping.

36. A. L. Schawlow and C. H. Townes, Phys. Rev. 112, 1940 (1958).

37. H. Risken, Ref. (3). We use the notation and evaluation of counting probabilities derived from Risken's work which appears in A. W. Smith and J. A. Armstrong, Phys. Rev. Letters 16, 1169 (1966).

38. Ref. (8), Eq. (47).

POLARIZATION AND ABSORPTION EFFECTS ON THE FRAUNHOFER DIFFRACTION PATTERNS OF A CORNER REFLECTOR

C. O. Alley, R. F. Chang, D. G. Currie, M. E. Pittman
University of Maryland, College Park, Maryland

I. INTRODUCTION

The far field diffraction pattern of a corner reflector will be considered, especially the effects of the relative phase shifts between different polarizations caused by total internal reflection. E. R. Peck[1] has studied the resultant state of polarization of the reflected light when a pencil of light falls upon one sector of the corner. M. M. Rao[2], following the method of Peck, has made a numerical study of the state of polarization for a corner reflector constructed of a particular type of glass. The eigen states of polarization predicted by Peck have been experimentally verified by Rabinowitz, et al[3]. A study, in terms of geometric optics, of the effects of angular errors in the prism on the return image has been made by P. R. Yoder, Jr.[4]. However, our present discussion shall assume that the corner is geometrically perfect; i.e., there are no angular errors in the corner reflector.

A beam of plane parallel monochromatic light falling upon a flat circular mirror produces in the far field the well-known Airy diffraction pattern. In the following we consider the far field pattern produced by combining the beams of different polarization which emerge from the six sectors of the corner reflector. The polarization and amplitude of each of these six beams is determined by the optical properties of the rear interface between the corner material and a metal or a dielectric,

i.e., the air or vacuum, as will be discussed in the following. In general, this pattern has more structure and angular divergence than the pattern which would be obtained if the corner reflector acted in the same manner as a flat mirror of the same diameter.

In more detail, each ray which "composes" the incident plane wave falling on the corner reflector is followed through a corner reflector in the manner of Peck, and the phase and amplitude of the ray emerging from the face of the corner reflector are determined. We thus neglect diffraction effects which occur inside the corner reflector. The phase shift and amplitude are determined by the optical properties of the rear surface; i.e., the glass-metal, glass-air, or air-metal interface. Each of these rear interfaces causes a relative phase shift between the components polarized parallel and perpendicular to the plane of incidence. An interface with a metal component also introduces a change in the amplitude of the wave. Our results will be compared to those for a "perfect" metal coating at the rear interface by which we mean an interface with the ideal properties of no change in amplitude and a relative change of phase between the parallel and perpendicular components of polarization of $-\pi$. (A material with infinite conductivity at optical frequencies would satisfy this criteria of "perfection".)

The amplitude and phase or, equivalently, the complex amplitudes thus determined have different values on the different sextants. In this computation, it has been assumed that the incident plane wave is approximately perpendicular to the front face. Rotating the corner reflector by an angle Φ would have two effects: (1) an overall change in the apparent shape of the front face (or the aperture) which would expand one axis of the resultant diffraction pattern, and (2) a change in the

angles of refraction at the rear interface, which would involve the charge of relative phase shifts with angle. The latter effect is second order in the angle Φ and thus small. The face of the corner reflector is assumed to be circular. Scalar diffraction theory is used to determine the far field pattern which results from all sextants with different complex amplitudes. The diffraction is calculated first for an arbitrary complex amplitude for each sector, and later the complex amplitudes are given the values which would result from a particular rear interface. The Fresnel reflection from the front face has been neglected. It would affect the diffraction pattern (apart from loss of intensity) only if the beam were exactly perpendicular to the front face.

The properties of specific interfaces are considered in Section V, and the diffraction patterns for silver, aluminum and total internal reflection are discussed. The metals have diffraction patterns rather similar to that of a "perfect" metal, and total internal reflection produces marked diffraction effects. In this section, some of the symmetries of the diffraction patterns are discussed.

In Section V, we present some photographs of the Fraunhofer diffraction pattern. These are seen to confirm the treatment and approximations made.

II. POLARIZATION AND INTENSITY EFFECTS OF A CORNER REFLECTOR ON A PENCIL OF LIGHT

A pencil of light which impinges axially upon one of the sextants of a corner reflector, after being reflected consecutively from three surfaces, emerges from the sextant opposite to the one it entered. As shown in Fig. 1, we designate by $\hat{i}$ and $\hat{j}$ the unit

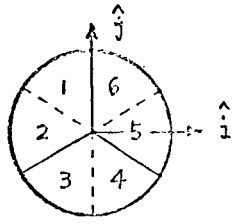

FIG. 1

IDENTIFICATION OF SEXTANT AND DESIGNATION OF POLARITIZATION OF COORDINATE VECTORS

Real Edges are indicated by solid lines, virtual edges are indicated by dotted lines.

vectors perpendicular and parallel, respectively, to the plane of incidence of the sextant labeled by 4. The light $\underset{\sim}{u} = \begin{pmatrix} u_1 \\ u_2 \end{pmatrix}$, where u_1 and u_2 are the complex amplitudes representing the phases and real amplitudes of the monochromatic light in the direction of $\hat{i}$ and $\hat{j}$ respectively, entering the sextant labeled by 4 would emerge from the sextant labeled by 1 with different complex components $u' = \begin{pmatrix} u'_1 \\ u'_2 \end{pmatrix}$. By tracing the ray through each reflection, it has been found[1] that $\underset{\sim}{u}$ and $\underset{\sim}{u}'$ can be related by a matrix $\underset{\sim}{C}$,

$$\underset{\sim}{u}' = \underset{\sim}{C}\,\underset{\sim}{u}.$$

The matrix $\underset{\sim}{C}$ has the form

$$\left.\begin{aligned} C_{11} &= \frac{1}{8} r_\perp \left[\left(r_\perp + r_\parallel \right)^2 + 4 r_\parallel \left(r_\perp - r_\parallel \right) \right] \\ C_{12} &= \frac{\sqrt{3}}{8} r_\parallel \left(r_\perp + r_\parallel \right)^2 \\ C_{21} &= \frac{\sqrt{3}}{8} r_\perp \left(r_\perp + r_\parallel \right)^2 \\ C_{22} &= \frac{1}{8} r_\parallel \left[4 r_\perp \left(r_\perp - r_\parallel \right) - \left(r_\perp + r_\parallel \right)^2 \right] \quad , \end{aligned}\right\} \qquad (1)$$

where $r_\perp$ and $r_\parallel$ are complex coefficients of reflectance which may be written as $r_\perp = \rho_\perp \exp(i\delta_\perp)$ and $r_\parallel = \rho_\parallel \exp(i\delta_\parallel)$. For total internal reflection $\rho_\perp = \rho_\parallel = 1$; otherwise, $\rho_\perp$ and $\rho_\parallel$ are less than unity representing reflection loss. Using the same polarization vectors for all sextants, we have six different matrices,

$$\underset{\sim}{u}^n = \underset{\sim}{C}^n \underset{\sim}{u}$$

where n = 1, 2, 3, 4, 5, and 6. The superscript n of the complex amplitude $\underset{\sim}{u}^n$ and the matrix $\underset{\sim}{C}^n$ is associated with the light emerging from n^{th} sextant. The matrix in Eq. (1) can now be identified as $\underset{\sim}{C}^1$ which is expressed in terms of Pauli's spin matrices, for the convenience of the following calculation, in the form

$$\underset{\sim}{C}^1 = \xi \underset{\sim}{1} + \sqrt{\tfrac{3}{2}}\, \eta \underset{\sim}{\sigma}_x + \zeta \underset{\sim}{\sigma}_y + \sqrt{\tfrac{1}{2}}\, \eta \underset{\sim}{\sigma}_z$$

where

$$\underset{\sim}{1} = \begin{pmatrix} 1 & 0 \\ 0 & 1 \end{pmatrix}, \quad \underset{\sim}{\sigma}_x = \begin{pmatrix} 0 & 1 \\ 1 & 0 \end{pmatrix}, \quad \underset{\sim}{\sigma}_y = \begin{pmatrix} 0 & -i \\ i & 0 \end{pmatrix}, \quad \underset{\sim}{\sigma}_z = \begin{pmatrix} 1 & 0 \\ 0 & -1 \end{pmatrix}$$

and

$$\left.\begin{aligned} \xi &\equiv \frac{1}{16}\left(r_\perp - r_{\shortparallel}\right)\left[3(r_\perp + r_{\shortparallel})^2 - 2(r_\perp - r_{\shortparallel})^2\right], \\ \eta &\equiv \frac{\sqrt{2}}{16}\left(r_\perp + r_{\shortparallel}\right)^3, \\ \zeta &\equiv -i\,\frac{\sqrt{3}}{16}\left(r_\perp + r_{\shortparallel}\right)^2\left(r_\perp - r_{\shortparallel}\right). \end{aligned}\right\} \qquad (2)$$

The matrices $\underset{\sim}{C}^3$ and $\underset{\sim}{C}^5$ can be obtained by rotating the matrix $\underset{\sim}{C}^1$ by the angles $\pm 120°$. Such a rotation may be accomplished by $\underset{\sim}{R}\underset{\sim}{C}\underset{\sim}{R}^{-1}$, yielding

$$\underset{\sim}{C}^3 = \frac{1}{4}\left(\underset{\sim}{1} + \sqrt{3}i\underset{\sim}{\sigma}_y\right)\underset{\sim}{C}^1\left(\underset{\sim}{1} - \sqrt{3}i\underset{\sim}{\sigma}_y\right)$$

$$= \xi\underset{\sim}{1} - \sqrt{\tfrac{3}{2}}\eta\underset{\sim}{\sigma}_x + \zeta\underset{\sim}{\sigma}_y + \sqrt{\tfrac{1}{2}}\eta\underset{\sim}{\sigma}_z \quad ,$$

$$\underset{\sim}{C}^5 = \frac{1}{4}\left(\underset{\sim}{1} - \sqrt{3}i\underset{\sim}{\sigma}_y\right)\underset{\sim}{C}^1\left(\underset{\sim}{1} + \sqrt{3}i\underset{\sim}{\sigma}_y\right)$$

$$= \xi\underset{\sim}{1} + \zeta\underset{\sim}{\sigma}_y - \sqrt{2}\eta\underset{\sim}{\sigma}_z \quad .$$

Matrices labeled by even numbers can be obtained by inverting $\underset{\sim}{C}^{7-n}$ with $\underset{\sim}{\sigma}_z$ because they make a mirror pair as far as the coordinate system is concerned,

$$\underset{\sim}{C}^n = \underset{\sim}{\sigma}_z\underset{\sim}{C}^{7-n}\underset{\sim}{\sigma}_z \quad , \quad n = 2, 4, \text{ and } 6.$$

This equation, because of the anticommutation relation of $\underset{\sim}{\sigma}$'s, results in simply changing of signs of the coefficients of $\underset{\sim}{\sigma}_x$ and $\underset{\sim}{\sigma}_y$ components. Consequently we can write $\underset{\sim}{C}^n$ in a general form as

$$\underset{\sim}{C}^n = \xi\underset{\sim}{1} + f_n\sqrt{\tfrac{1}{2}}\eta\underset{\sim}{\sigma}_x + g_n\zeta\underset{\sim}{\sigma}_y + h_n\sqrt{\tfrac{1}{2}}\eta\underset{\sim}{\sigma}_z \quad . \tag{3}$$

The coefficients f_n, g_n and h_n are tabulated in Table I for all sextants.

n	f_n	g_n	h_n
1	1	1	1
2	0	-1	-2
3	-1	1	1
4	1	-1	1
5	0	1	-2
6	-1	-1	1

TABLE I

The coefficients in the transmission matrices

As indicated by the form of the transmission matrices $\underset{\sim}{C}^n$, the polarization and amplitude of the entering light is, in general not preserved. One can, however, use projection operators to decompose the emerging beam into two polarization components along directions other than $\hat{i}$ and $\hat{j}$. In particular we will consider one

component parallel to the incident polarization and the other perpendicular to it. Assume the impinging ray is linearly polarized in the direction such that it makes an angle θ with $\hat{i}$ as shown in Fig. 2, so it has the form $\underset{\sim}{u} = u_o \begin{pmatrix}\cos\theta \\ \sin\theta\end{pmatrix}$. The eigenvectors of these projection operators are,

$$\underset{\sim}{v}_{\shortparallel} = \begin{pmatrix}\cos\theta \\ \sin\theta\end{pmatrix} \text{ and } \underset{\sim}{v}_{\perp} = \begin{pmatrix}\sin\theta \\ -\cos\theta\end{pmatrix}$$

respectively for the components parallel and perpendicular to the incident polarization. Thus the normalized complex amplitudes of the emerging light from n^{th} sextant for these two components are,

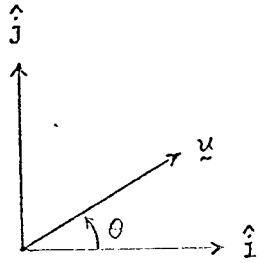

FIG. 2
Assumed Polarization State of Incident Light.

$$\left.\begin{aligned}
\gamma_{\shortparallel}^{n} &= \underset{\sim}{v}_{\shortparallel}^{\dagger}\, \underset{\sim}{C}^{n}\, \underset{\sim}{u} / \sqrt{\underset{\sim}{u}^{\dagger}\underset{\sim}{u}} \\
&= \xi + f_n \sqrt{\tfrac{3}{2}}\eta \sin 2\theta + h_n \sqrt{\tfrac{1}{2}}\eta \cos 2\theta \\
\gamma_{\perp}^{n} &= \underset{\sim}{v}_{\perp}^{\dagger}\, \underset{\sim}{C}^{n}\, \underset{\sim}{u} / \sqrt{\underset{\sim}{u}^{\dagger}\underset{\sim}{u}} \\
&= -g_n i\zeta + h_n \sqrt{\tfrac{1}{2}}\eta \sin 2\theta - f_n \sqrt{\tfrac{3}{2}}\eta \cos 2\theta.
\end{aligned}\right\} \quad (4)$$

The polarization properties of the emergent beam are determined by the phase between $\gamma_{\shortparallel}^{n}$ and $\gamma_{\perp}^{n}$ which in turn may be expressed as functions of $r_{\shortparallel}$ and $r_{\perp}$, the complex coefficients of reflectance. Similarly, intensity properties of the emergent beam are related to $r_{\shortparallel}$ and $r_{\perp}$ by the expression $\left|\gamma_{\shortparallel}^{n}\right|^2 + \left|\gamma_{\perp}\right|^2$.

III. DIFFRACTION PATTERN FOR A SIX-SECTORED CIRCLE WITH ARBITRARY PHASES AND AMPLITUDES

For a single polarization the integral governing Fraunhofer diffraction is[5]

$$U(P) = B\iint_S e^{-ik(p\alpha + q\beta)}\, d\alpha\, d\beta, \tag{5}$$

where U (P) is the amplitude at point P, p and q are defined as the difference of the direction cosines between the point of observation P and that of the direction of incidence. The region of integration is the area of the aperture S. The constant B in front of the integral in Eq. (5) expresses the intensity and phase of the emerging light which are constant over the whole area S. If, as a simple example, the phase and amplitude are the same in each of the sextants, then the result is the well-known diffraction pattern for a circle of radius a,

$$U(P) = B\int_0^a\int_0^{2\pi} e^{-ik\rho w\cos(\phi-\psi)}\rho\, d\rho\, d\phi$$

$$= B\pi a^2\,\frac{2J_1(kaw)}{kaw}\quad, \tag{6}$$

where a new set of coordinates (w,ψ) were introduced to describe the points on the plane of observation replacing (p,q); and (ρ,ϕ) were introduced to describe the points on the region of integration replacing (α,β). These are obtained by the transformation[5]

$$w\cos\psi = p, \quad w\sin\psi = q. \quad \text{and}$$

$$\rho\cos\phi = \alpha, \ \rho\sin\phi = \beta\quad .$$

Here w is the sine of the angle which the direction (p,q) makes with the central direction p = q = 0. The diffraction pattern for the circular hole is circularly symmetric and is independent of ψ. But if we consider the case of the light emerging from a six-sectored circle with different phase and amplitude for each sextant, as in Fig. 3, the diffraction pattern loses its simple form and, in general, the integral depends on the angle ψ. Because of the kind of transformation we made above, this polar angle ψ is measured from the same axis as ϕ is measured, that is, counter-clockwise from $\hat{j}$-axis when facing the source of radiation. Using the same new coordinates as in Eq. (6)., the diffraction integral over the six-sectored circle then becomes

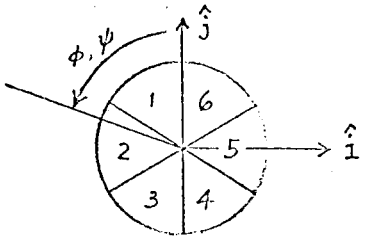

FIG. 3
Zero Line of Polar Angle ψ.

$$U(P) = \sum_{n=1}^{6} B_n \int_0^a \int_{(n-1)\pi/3}^{n\pi/3} e^{-ik\rho w \cos(\phi-\psi)} \rho d\rho d\phi ,$$

where the B_n describes the phase and amplitude of the light of a particular polarization coming from each sextant of the circle. It is assumed that the phase and amplitude is constant over a given sextant. Since our interest is in the distribution of the energy, we can normalize the amplitude such that in the case of a circular "perfect" mirror, which is perpendicular to the direction of incidence the central intensity $I_o = |U(0,0)|^2$ is unity. This yields

$$A(P) = \frac{1}{\pi a^2} \sum_{n=1}^{6} \gamma^n \int_0^a \int_{(n-1)\pi/3}^{n\pi/3} e^{-ik\rho w \cos(\phi-\psi)} \rho d\rho d\phi \qquad (7)$$

where A(P) is the normalized complex amplitude of the diffraction and γ^n is the normalized complex amplitudes of the n^{th} sextant.

To evaluate the integral in Eq. (7), we use the formulas[6]

$$\cos\ (z\cos\theta) = J_o(z) + 2\sum_{k=1}^{\infty} (-)^k J_{2k}(z)\cos(2k\theta)$$

$$\sin\ (z\cos\theta) = 2\sum_{k=1}^{\infty} (-)^k J_{2k}(z)\cos[(2k+1)\theta]\ ,$$

where $J_{2k}(z)$ are the Bessel functions, to separate the radial and angular parts in the integral. After evaluating the angular part, we obtain

$$A(P) = \frac{1}{\pi x^2}\sum_{n=1}^{6}\gamma^n\int_o^x y\,dy\,[\tfrac{\pi}{3}J_o(y) + 4\sum_{\ell=1}^{\infty}\frac{(-i)^\ell}{\ell}J_\ell(y)\sin\tfrac{\ell\pi}{6}\cos\{\ell(\tfrac{n\pi}{3} - \psi - \tfrac{\pi}{6})\}] \quad (8)$$

where $x \equiv kaw$, $y \equiv k\rho w$.

It is well known that

$$\int_o^x y\,J_o(y)\,dy = xJ_1(x), \quad (9)$$

but the second integral which involves higher orders of the Bessel functions can be expressed in terms of the Bessel functions or in a power series of x. In either case the series converges rather quickly, and has the form[6]

$$\int_o^x y\,J_\ell(y)\,dy = 2\ell x\sum_{m=0}^{\infty}\frac{(\ell+2m+1)}{(\ell+2m+2)(\ell+2m)}J_{\ell+2m+1}(x) \quad (10)$$

or

$$\int_o^x yJ_\ell(y)\ dy = 4\left(\frac{x}{2}\right)^{\ell+2} \sum_{m=0}^{\infty} \frac{(-x^2/4)^m}{(\ell + 2m + 2)(m!)(\ell + m)!} \qquad (11)$$

For $\ell = 0$, both Eqs. (10) and (11) will reduce to Eq. (9), noticing $J_1(x) = \frac{x}{2} \sum_{m=0}^{\infty} \frac{(-x^2/4)^m}{m!\ (m + 1)!}$ in the case of Eq. (11).

Since the integral is well-determined, we can, for short, define a new function $F_\ell(x)$ as in the following:

$$F_\ell(x) \equiv \frac{1}{\ell x^2} \int_o^x y\ J_\ell(y)\ dy \quad . \qquad (12)$$

Then the Eq. (8) can be rewritten as

$$A(P) = \frac{2J_1(x)}{x} \sum_{n=1}^{6} \frac{\gamma^n}{6} + \frac{4}{\pi} \sum_{\ell=1}^{\infty} (-i)^\ell\ F_\ell(x)\ \sin\frac{\ell\pi}{6} \sum_{n=1}^{6} \gamma^n \cos\left[\ell\left(\frac{n\pi}{3} - \psi - \frac{\pi}{6}\right)\right].$$

(13)

In the case of a "perfect" mirror, all γ^n's are equal to unity, (omitting the common phase;) then $\sum_{n=1}^{\infty} \gamma^n/6 = 1$ plus

$$\sin\frac{\ell\pi}{6} \sum_{n=1}^{6} \cos\left[\ell\left(\frac{n\pi}{3} - \phi\right)\right] \equiv 0$$

for all ℓ and ϕ, consequently Eq. (13) reduces to the form of Eq. (6) as we expected.

This discussion has been for a single polarization. In general, (and for the corner reflector in particular) the polarization from each of the sextants may not be the same. Since beams of orthogonal polarization do not interfere, we may calculate the diffraction pattern due to each polarization, calculate the intensities due to each polarization, and then add the intensities. Although this may be done for a resolution into any pair of orthogonal polarization states, we will find it convenient to consider orthogonal linear polarizations.

IV. DIFFRACTION PATTERNS AS A FUNCTION OF THE REFLECTING SURFACE

The results of the last section are expressed in terms of the phase and amplitude of the light on each sextant. If the light was originally plane parallel light of uniform intensity, then the phase and amplitude of each sextant may be expressed as a function of the phase and absorption at a glass-metal or glass-air interface at the angle which occurs in the corner reflector. This was done in Section II. We may now use Section II to express the diffraction pattern in terms of the characteristic of the interface.

We again treat each of the outgoing polarizations separately. First we substitute the value of $\gamma_{\parallel}^{n}$ and $\gamma_{\perp}^{n}$ obtained from Eq. (4) into Eq. (13) and then sum over n from 1 to 6. After somewhat lengthy algebraic calculation we obtain the expression of the normalized amplitude for both polarizations to be

$$A_{\parallel}(x,\psi;\Theta) = \xi \frac{2J_1(x)}{x} + \eta \frac{6\sqrt{6}}{\pi} \sum_{\ell=1}^{2} \sum_{m=0}^{\infty} (-)^{m+1} F_{2\ell+6m}(x) \cos[(2\ell+6m)\psi+(-)^{\ell}2\Theta] , \tag{14}$$

$$A_{\perp}(x,\psi;\Theta) = \zeta \frac{24}{\pi} \sum_{m=0}^{\infty} (-)^{m} F_{3+6m}(x) \sin(3+6m)\psi$$

$$+ \eta \frac{6\sqrt{6}}{\pi} \sum_{\ell=1}^{2} \sum_{m=0}^{\infty} (-)^{m+\ell-1} F_{2\ell+6m}(x) \sin[(2\ell + 6m)\ \psi + (-)^{\ell}\ 2\Theta]. \tag{15}$$

It is interesting to note that the diffraction pattern of a corner reflector depends solely on four basic functions regardless of the property of the reflecting surface. The difference in the properties of the reflecting surfaces shows in the values of ξ, η and ζ which affect only the strengths of these four functions.

We can now define four G- functions $G_0(x)$, $G_1(x,\psi;\theta)$, $G_2(x,\psi)$ and $G_3(x,\psi;\theta)$ as in the following.

$$G_0(x) = \frac{2J_1(x)}{x} \tag{16}$$

$$G_1(x,\psi;\theta) = \frac{6\sqrt{6}}{\pi} \sum_{\ell=1}^{2} \sum_{m=0}^{\infty} (-)^{m+1} F_{2\ell+6m}(x) \cos[(2\ell+6m)\psi + (-)^{\ell} 2\theta] \tag{17}$$

$$G_2(x,\psi) = \frac{24}{\pi} \sum_{m=0}^{\infty} (-)^{m} F_{3+6m}(x) \sin(3 + 6m)\psi \tag{18}$$

$$G_3(x,\psi;\theta) = \frac{6\sqrt{6}}{\pi} \sum_{\ell=1}^{2} \sum_{m=0}^{\infty} (-)^{m+\ell-1} F_{2\ell+6m}(x) \sin[(2\ell + 6m)\psi + (-)^{\ell} 2\theta]. \tag{19}$$

Then Eqs. (14) and (15) can be rewritten as

$$A_{\parallel} = \xi G_0(x) + \eta G_1(x,\psi;\theta) \tag{20}$$

$$A_{\perp} = \zeta G_2(x,\psi) + \eta G_3(x,\psi;\theta) \tag{21}$$

Thus both amplitudes may be expressed as combinations of the G-functions.

A computer calculation of these functions could be made to give the detailed diffraction patterns for any type of corner reflector, but this will not be done in the present paper.

We are also interested in the energy which lies within a given angular radius of the center of the beam. Let L(w) denote the fraction of the total energy which lies within an angular radius w. Thus we have

$$L(w) = \frac{\pi a^2}{\lambda^2} \int_0^{2\pi} \int_0^{w} I(w', \psi; \Theta)\, w'\, dw'\, d\psi \quad , \tag{22}$$

where $\lambda = 2\pi/k$ is the wavelength of the light. The intensity is given by

$$I(w, \psi; \Theta) = |A_{\perp}(x, \psi; \Theta)|^2 + |A_{\parallel}(x, \psi; \Theta)|^2$$

where x = kaw as before.

Using Eqs.(20) and (21), we get

$$\begin{aligned} I(w, \psi; \Theta) = {} & |\xi|^2 G_0^2(x) + (\xi\eta^* + \xi^*\eta) G_0(x) G_1(x, \psi; \Theta) + |\eta|^2 G_1^2(x, \psi; \Theta) \\ & + |\zeta|^2 G_2^2(x, \psi) + (\zeta\eta^* + \zeta^*\eta) G_2(x, \psi) G_3(x, \psi; \Theta) + |\eta|^2 G_3^2(x, \psi; \Theta) \end{aligned} \tag{23}$$

Noting that the angular integration cancels the cross terms, we may

calculate each term to obtain

$$L(w) = 2|\xi|^2 \int_0^x \frac{J_1^2(x')}{x'}\,dx' + \frac{108}{\pi^2}|\eta|^2 \sum_{\ell=1}^{2}\sum_{m=0}^{\infty} \int_0^x F^2_{2\ell+6m}(x')x'dx'$$

$$+ \frac{144}{\pi^2}|\zeta|^2 \sum_{m=0}^{\infty} \int_0^x F^2_{3+6m}(x')x'dx'$$

The energy within the first zero of the Airy disc is given by $L(w_o)$, where $w_o = 3.83/ka$. Evaluating the above expressions, this yields

$$L(w_o) = 0.84|\xi|^2 + 0.44|\eta|^2 + 0.06|\zeta|^2 \quad . \tag{24}$$

As an simple illustration, let us consider the values of the parameters such that the reflection surface of a corner reflector acts as an "perfect" mirror. These are given by conditions

$$\left.\begin{aligned} r_\perp + r_\parallel &= 0 \\ \text{and} \qquad\qquad & \\ r_\perp - r_\parallel &= 2\exp(i\delta_\perp) \quad . \end{aligned}\right\} \tag{25}$$

Substituting these values into Eq. (2), we obtain

$$\xi = -\exp(i3\delta_\perp) \text{ and } \eta = \zeta = 0.$$

This result reduces Eqs. (20) and (21) to what we expect from a circular aperture, that is

$$A_\parallel = -\exp(i3\delta_\perp)\frac{2J_1(x)}{x}, \quad A_\perp = 0 \quad .$$

Thus a corner reflector whose back surfaces act as a "perfect" mirror has the same diffraction pattern as a "perfect" flat circular mirror.

V. EXPECTED PATTERNS FROM CORNER REFLECTORS COATED WITH ALUMINUM, SILVER, UNCOATED, AND OPEN CORNER REFLECTORS

Since the diffraction pattern of a corner reflector is a linear combination of the four G-functions, we need only calculate the strength coefficients ξ, η and ζ of different coatings (See Appendix). The cases considered are uncoated solid corner reflectors as well as reflectors coated with aluminum, and with silver. In addition, open corner reflectors having aluminum and silver as reflecting surfaces are considered. As an illustration, the strength coefficients ξ, η, ζ and some other related quantities are tabulated in Table II. There, the wavelength of the light considered is 6943 Å which is the value of the ruby pulse laser. The index of refraction of the glass of the solid corner reflector is assumed to be 1.5 (approximately the index of fused silicon). The index of refraction n and the absorption coefficient k of the metals were taken from Schulz and Tangherlini[7,8].

We also examine the reflection loss of a corner reflector. Let E_{in} denote the total energy entering the reflector and E_{out} the total energy returning from it. Then, rather than integrate the diffraction intensity we can calculate E_{out} by using the matrices introduced in Section II.

The ratio of energy is $E_{out}/E_{in} = \frac{1}{6} \sum_{n=1}^{6} \underset{\sim}{u}^{\dagger} \underset{\sim}{C}^{n\dagger} \underset{\sim}{C}^{n} \underset{\sim}{u} / \underset{\sim}{u}^{\dagger} \underset{\sim}{u}$.

Noticing

$$\sum_{n=1}^{6} f_n = \sum_{n=1}^{6} g_n = \sum_{n=1}^{6} h_n = \sum_{n=1}^{6} f_n g_n = \sum_{n=1}^{6} g_n h_n = \sum_{n=1}^{6} h_n f_n = 0$$

from Table I, we obtain

$$E_{out}/E_{in} = \frac{1}{6} \sum_{n=1}^{6} \left[|\xi|^2 + \frac{3}{2} f_n^2 |\eta|^2 + g_n^2 |\zeta|^2 + \frac{1}{2} h_n^2 |\eta|^2 \right]$$

$$= |\xi|^2 + 2|\eta|^2 + |\zeta|^2 .$$

Since the fraction of energy distributed in $G_o(x)$ alone is $|\xi|^2$, we can conclude that the extra terms $2|\eta|^2$ and $|\xi|^2$ are the fractions of energy distributed in $G_1(x,\psi;\Theta)$, $G_3(x,\psi;\Theta)$ and $G_2(x,\psi)$. The energy ratio (E_{out}/E_{in}) of different cases considered are listed in Table II.

The fractional energy contained within the first zero of $G_o(x)$, as given in Eq. (24), is also listed in Table II for the cases considered.

	Solid Corner Reflector with Back Coating *		Open Corner Reflector		Total Internal Reflection
	Ag	Al	Ag	Al	n=1.5
$\rho_\perp^2$	0.989	0.906	0.992	0.937	1.0
$\rho_\parallel^2$	0.970	0.750	0.978	0.824	1.0
$\|\xi\|^2$	0.929	0.562	0.953	0.603	0.290
$\|\eta\|^2$	7.750×10^{-4}	0.466×10^{-4}	0.944×10^{-4}	0.047×10^{-4}	0.316
$\|\zeta\|^2$	8.676×10^{-3}	1.208×10^{-3}	2.290×10^{-3}	0.268×10^{-3}	0.079
$L(w_o)$	78.1%	47.2%	80.1%	50.7%	39.0%
E_{out}/E_{in}	93.9%	56.3%	95.6%	60.4%	100%

Table II Calculated expectations of energy concentration

* Reflection loss at the front surface is neglected in the use of solid corner reflectors.

In Fig. 4 the diffraction patterns taken from an uncoated corner reflector are shown. Since the polarization angle θ is chosen to be zero, three of the four G-functions with angular dependence reduce to a simpler form of

$$G_1(x,\psi;0) = \frac{6\sqrt{6}}{\pi} \sum_{\ell=1}^{2} \sum_{m=0}^{\infty} (-)^{m+1} F_{2\ell+6m}(x) \cos[(2\ell + 6m)\psi] \quad (26)$$

$$G_2(x,\psi) = \frac{24}{\pi} \sum_{m=0}^{\infty} (-)^{m} F_{3+6m}(x) \sin[(3 + 6m)\psi] \quad (27)$$

$$G_3(x,\psi;0) = \frac{6\sqrt{6}}{\pi} \sum_{\ell=1}^{2} \sum_{m=0}^{\infty} (-)^{m+\ell-1} F_{2\ell+6m}(x) \sin[(2\ell + 6m)\psi]. \quad (28)$$

In Fig. 4a the symmetries of the pattern are: (1) "up to down" symmetry corresponding to "ψ to $-\psi$" symmetry in intensity $I_{\shortparallel}(x,\psi;0)$, (2) "left to right" symmetry corresponding to "ψ to $\pi-\psi$" symmetry.* Now we examine Eq.(26) which is responsible for the angular dependence of $A_{\shortparallel}(x,\psi;0)$. Since $G_1(x,\psi;0)$ contains $\cos[(2\ell + 6m)\psi]$, one sees that

$$\cos[(2\ell + 6m)(-\psi)] = \cos[(2\ell + 6m)\psi],$$

and

$$\cos[(2\ell + 6m)(\pi-\psi)] = \cos[(2\ell + 6m)\pi-(2\ell + 6m)\psi]$$
$$= \cos[(2\ell + 6m)\psi]$$

would assure that

$$G_1(x,\psi;0) = G_1(x,-\psi;0) = G_1(x,\pi-\psi;0).$$

* These two symmetries would automatically include ψ to $\psi+\pi$ symmetry, i.e., invertion through the origin.

Consequently the amplitude distribution function

$$A_{\parallel}(x,\psi;0) = \xi G_o(x) + \eta G_1(x,\psi;0)$$

obeys the same symmetry.

In Fig. 4b the pattern does not possess as high the symmetry as that of Fig. 4a. The only symmetry displayed here is "up to down" symmetry corresponding to "ψ to $-\psi$" symmetry. Examining Eqs. (27) and (28) one sees that $G_2(x,\psi)$ and $G_3(x,\psi;0)$ contain $\sin[(3 + 6m)\psi]$ and $\sin[(2\ell + 6m)\psi]$, respectively. Under the operation of "ψ to $-\psi$" both terms change sign simultaneously, changing only the phase of the field $A_{\perp}(x,\psi;0)$ by 180°. Consequently the intensity, $I_{\perp}(x,\psi;0) = A_{\perp}^{*}(x,\psi;0)A_{\perp}(x,\psi;0)$, would remain symmetric.

In addition to the symmetry property, Fig. 4b shows several dark lines. One of these is the horizontal line going through the origin. This line corresponds to ψ=0. Inserting ψ=0 in Eqs. (29) and (28) we get $G_2(x,0) = 0$, $G_3(x,0;0) = 0$, and so vanishes the amplitude $A_{\parallel}(x,0;0)$. There are also two sections of dark lines passing through origin at the angles $\psi = \pm\pi/3$. Inserting $\psi = \pm\pi/3$ into Eq. (27) one finds that $G_2(x,\pm\pi/3) = 0$ whereas $G_3(x, \pm\pi/3;0)$ does not. Therefore the intensity along the line $\psi = \pm\pi/3$ is contributed only by $G_3(x,\pm\pi/3;0)$, it is less intense than its near neighborhood where both $G_2(x,\psi)$ and $G_3(x,\psi;0)$ contribute. Finally one notices the dark origin. To verify this one must review the Eqs. (11) and (12). Combining these two equations we get

$$F_{\ell}(x) = \frac{1}{\ell}\left(\frac{x}{2}\right)^{\ell}\sum_{m=0}^{\infty}\frac{\left(-\frac{x^2}{4}\right)^m}{(\ell+2m+2)(m!)(\ell+m)!} \qquad (29)$$

where ℓ is any positive integer. This Eq. (35) shows that $F_\ell(0)=0$. Therefore $G_2(0,\psi)$ and $G_3(0,\psi;0)$ vanish, leaving a dark point at the center.

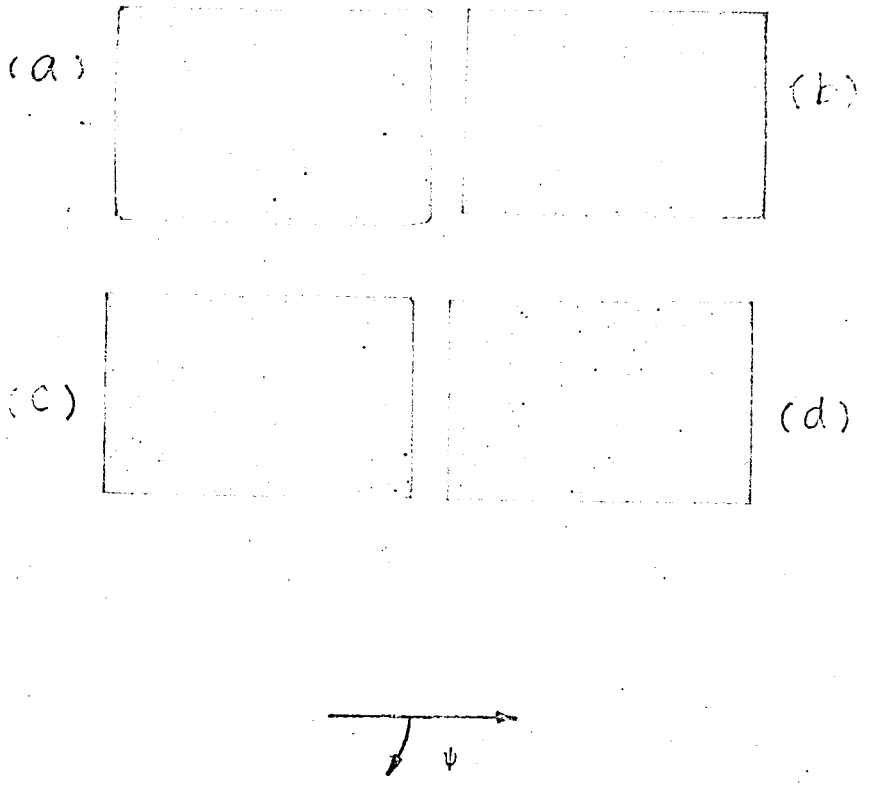

FIG. 4

DIFFRACTION PATTERNS

An uncoated corner reflector was used to demonstrate the polarization effect. The incident beam was polarized along the $\hat{i}$-axis such that the angle $\theta=0$. The corner reflector has the front face of 1 1/2 inch in diameter. (a) Diffraction pattern from a flat mirror with the same aperture as the corner reflector. (b) Total diffraction pattern from the corner reflector. (c)Diffraction pattern which has the polarization parallel to the incident beam. (d) Diffraction pattern which has the polarization perpendicular to the incident beam.

VI. CONCLUSION AND THE COMMENT

In this study of the far field diffraction pattern for a corner reflector, we considered, among other things, mainly the energy concentration at the central region.

The purpose of this particular consideration is to investigate the possibility of ranging the moon with an optical radar system on the ground and the corner reflectors on the moon. Thus quantitative information on the concentration of the returning signal is the primary interest.

The diffraction pattern from a circular aperture illuminated uniformly by a plane wave contains about 84% of its energy within the angular radius of $1.22\ \lambda/d$, where d is the diameter of the aperture. For a corner reflector, however, when the total internal reflection is employed to minimize the reflection loss, the diffraction pattern of the returning beam contains less than half of the energy in the same angular radius as compared to the circular aperture. It is because the polarization effects manifests itself to a greater extent in the total internal reflection. There is little tendency that the field at points far away from the central region would be cancelled as it would be in the case of circular aperture. The consequence is a greater spread of energy. Coating the back surfaces of the corner reflector with metals would generally improve the performance in the sense that more energy would tend to concentrate in the central region. But the absorption by the metal would reduce

the returning intensity. The light entering a corner reflector has to be reflected three times before emerging, thus the desirability of high reflectance at the reflecting interface is greatly signified.

The particular geometry of the corner reflector predetermined the basic structure of its diffraction pattern as a combination of four functions. The different optical constants of the different reflecting interfaces provide merely the different strength coefficients for each of these four functions, namely ξ, η and ζ. Three of these four functions do not diminish rapidly as the argument increases. Therefore the high value of the strength coefficients of these three functions, namely η and ζ, would result in the wider spread of the energy.

The use of metals such as silver and aluminum on the back surfaces of a corner reflector would reduce the polarization effects to such an extent that $|\eta|^2$ and $|\zeta|^2$ is negligibly small. But $|\xi|^2$ may or may not be near to unity. Particularly the angle of incidence under consideration is in the neighborhood of the "principle angle of incidence" of the metals. The reflectance $\rho_{\perp}^2$ is near minimum. Therefore the coefficient $|\xi|^2$ which goes roughly as $\rho_{\perp}^3$ is seriously effected. In order to obtain the highest possible value of $|\xi|^2$, the use of highly reflective metals are most desirable. The metal such as silver is certainly a good choice.

REFERENCES

1. E. R. Peck, J. Opt. Soc. Am. 52, 253 (1962).

2. M. M. Rao, Department of Optics, University of Rochester, Rochester, New York, 1963.

3. P. Rabinowitz, S. F. Jacobs, T. Shultz, G. Gould, J. Opt. Soc. Am. 52, 452 (1962).

4. P. R. Yoder, Jr., J. Opt. Soc. Am. 48, 496 (1958).

5. Born and Wolf, Principles of Optics, 2nd Revised edition (Macmillan Co., New York), 1964.

6. Abramowitz and Stegun, Handbook of Mathematical Functions, (Dover, New York), 1965.

7. L. G. Schulz, J. Opt. Soc. Am. 44, 357 (1954).

8. L. G. Schulz and F. R. Tangherlini, J. Opt. Soc. Am 44, 362 (1954).